Direct sensitivity analysis of multibody systems with holonomic and nonholonomic constraints via an index-3 augmented Lagrangian formulation with projections

Daniel Dopico, Francisco González, Alberto Luaces,

Mariano Saura, Daniel García-Vallejo

This is a post-peer-review, pre-copyedit version of an article published in Nonlinear Dynamics. The final authenticated version is available online at:

http://dx.doi.org/10.1007/s11071-018-4306-y.

Abstract

Optimizing the dynamic response of mechanical systems is often a necessary step during the early stages of product development cycle. This is a complex problem that requires to carry out the sensitivity analysis of the system dynamics equations if gradient-based optimization tools are used. These dynamics equations are often expressed as a highly nonlinear system of Ordinary Differential Equations (ODEs) or Differential-Algebraic Equations (DAEs), if a dependent set of generalized coordinates with its corresponding kinematic constraints is used to describe the motion. Two main techniques are currently available to perform the sensitivity analysis of a multibody system, namely the direct differentiation and the adjoint variable methods.

In this paper, we derive the equations that correspond to the direct sensitivity analysis of the index-3 augmented Lagrangian formulation with velocity and acceleration projections. Mechanical systems with both holonomic and nonholonomic constraints are considered. The evaluation of the system sensitivities requires the solution of a Tangent Linear Model (TLM) that corresponds to the Newton-Raphson iterative solution of the dynamics at configuration level, plus two additional nonlinear systems of equations for the velocity and acceleration projections. The method was validated in the sensitivity analysis of a set of examples, including a five-bar linkage with spring elements, which had been used in the literature as

benchmark problem for similar multibody dynamics formulations, a point-mass system subjected to nonholonomic constraints, and a full-scale vehicle model.

Keywords: Sensitivity analysis, Multibody system dynamics, Index-3 augmented Lagrangian method

1 Introduction

During the last decades many different formulations of the equations of motion of multibody systems have been derived using several coordinate sets [40, 45, 46, 33, 23]. Because sensitivity analysis of the dynamics is essential for gradient-based design optimization and optimal control, the sensitivity equations for several of these formulations have been derived too, in parallel to the evolution of multibody dynamics techniques. Dynamic sensitivities, when needed, are often calculated by means of finite differences but this procedure can be very demanding in terms of time and the accuracy poor in many cases, especially if real finite differences are used [19]. Other strategies to obtain them include the use of detailed analytical expressions [20, 19], symbolic differentiation [2], or automatic differentiation [9, 10]. Two main methods have been employed in the literature for the analytical calculation of sensitivities: forward differentiation and the adjoint variable method [11].

As a general rule, a set of dependent coordinates is needed to write the dynamic equations of complex systems and, assuming that these dependent coordinates are related by a set of holonomic rheonomic constraint equations, the basic form of the dynamics equations is usually admitted to be a system of index-3 Differential-Algebraic equations (DAE system). In the early days of multibody dynamics, the sensitivity equations for the index-3 DAE formulation were derived, [32]. Unfortunately, the direct solution of the index-3 DAE entails some numerical difficulties [8, 28] that make it convenient to reformulate the problem in some way. Since the underlying formulation of the equations of motion is generally not useful to solve general problems in multibody dynamics, the sensitivity equations cannot be considered useful in many cases either. In [19] the sensitivity equations of the index-3 DAE formulation were derived as a basis for more complex formulations. A stability analysis of the adjoint sensitivity equations was also presented in [41].

Most of the contemporary methods to reformulate the original DAE include one or more

of the following techniques [3] to deal with the algebraic constraints present in the system: reducing the index and stabilizing the original DAE [4, 27]; removing the constraints by writing the equations of motion in the configuration space [44, 47]; adding penalty or augmented Lagrangian terms [5]; or using projections onto the constraint manifolds [6, 21, 13]. The aforementioned possible choices of coordinates and techniques to write the equations of motion, along with the different time-stepping schemes available to integrate the equations of motion, give rise to the vast amount of methods proposed in the bibliography for the forward dynamics of multibody systems [23].

The most popular alternative based on index reduction is the Lagrange index-1 formulation[23]. Some authors have derived and proposed the use of this formulation for sensitivity analysis of multibody systems [7, 15, 42]. This method, however, suffers from drift-off [21] and it is not able to deal with redundant constraints and singular configurations, very common in multibody systems. These reasons have led to the development of more advanced formulations that do not suffer from the above mentioned problems.

In order to circumvent the drift-off-effect of the Lagrange index-1 formulation, [4] proposed a stabilization technique for the constraints. The sensitivity equations for Baumgarte's formulation were derived in [12] and used for design optimization. Although this formulation solves the drift-off problem, it introduces some amount of numerical damping in the solutions and it is still not able to deal with redundant constraints and singular configurations.

In [5] the penalty method in the context of multibody dynamics was introduced. The formulation solves the problems mentioned before for index-3 and index-1 formulations and reduces the dynamics equations to a system of ordinary differential equations (ODE), instead of the original DAE. The sensitivity equations for this formulation are also available in [37, 38, 19] and they were even used for the dynamic optimization of a whole vehicle in [48]. Accordingly the penalty method is a good candidate for the optimization of industrial problems. The solutions of its dynamics equations are equivalent to the original DAE for infinite penalty factors, but in floating point computing loss-of-significance errors and ill-conditioning appear for large penalties. Thus, the selection of the penalty factors is a sensitive issue that the analyst has to face and, moreover, the formulation tends to dissipate a non-negligible amount of energy. These difficulties point to the need for more advanced formulations for both dynamics and sensitivities.

Another option is deriving the sensitivity equations of multibody formulations based on in-

dependent coordinates: in [1] the dynamics sensitivities based on Kane equations [34] were covered; in [20], the sensitivity analysis using the Matrix R formulation was accomplished; in [31] the sensitivity analysis of the recursive Maggi's formulation was solved.

The consideration of nonholonomic constraints in the system makes the problem more complex and requires special methods to deal with them, as pointed out in [43], with the use of the virtual power principle [34, 23] for formulations in minimal coordinates. In the case of formulations in dependent coordinates, the use of special penalty terms was proposed in [5] to consider nonholonomic constraints in the framework of an augmented Lagrangian formulation. The Index-3 Augmented Lagrangian formulation with Projections (ALI3-P formulation) for holonomic and nonholonomic systems presented in [16] outperforms the behavior of the precedent penalty and augmented Lagrangian formulations in [5], sharing the advantages of those and removing many of their drawbacks. It represents the extension of the formulations presented in [6, 13] to nonholonomic systems and their generalization to more advanced integration schemes. This formulation constitutes a good exponent of what it should be expected from a modern multibody method: it is efficient, accurate, and robust; it exactly satisfies the constraints at position, velocity, and acceleration levels; it has predictable and controllable energy decaying properties [26, 24, 25]; it can deal with redundant constraints and singular configurations without special considerations [29] and it can handle both holonomic (scleronomic and rheonomic) and nonholonomic constraints.

A considerable number of non-academic multibody systems are currently solved using the ALI3-P formulation, since complex phenomena like contact with friction and tire forces [17, 39], flexible bodies [14], or even multiphysics [35] can be naturally accommodated to the formulation. Given the fact that the evaluation of the sensitivity equations relies on the previous solution of the forward dynamics, obtaining the sensitivity equations for the ALI3-P formulation is a valuable contribution for the optimization and control of such systems. In general, it is advisable, and more rigorous, to use the same formulation for dynamics and sensitivity analysis. For instance, if a forward-dynamics simulation has been carried out using the ALI3-P method, using the Matrix R approach to evaluate the sensitivity terms would require the evaluation of the velocity transformation terms and their derivatives at each integration time-step, with the corresponding computational overhead. Moreover, the Matrix R method does not explicitly provide constraint reactions, and so the objective function could not be explicitly dependent on them, a problem that does not affect the ALI3-P formulation.

The sensitivity equations of the ALI3-P formulation derived in this work are novel and present important differences with respect to their counterparts for the formulations already developed in [20, 19]. In particular, the derivation of the sensitivities of the projections onto the constraint manifolds is a significant contribution of this work. This paper also shows that correctly evaluating the sensitivity of the projections is crucial to obtain accurate solutions in systems with nonholonomic constraints. The properties of the newly proposed method have been compared to those of existing ones in terms of accuracy, stability, and efficiency in the sensitivity analysis of a set of examples.

2 The ALI3-P formulation for systems with nonholonomic constraints

The equations of motion of the ALI3-P formulation were thoroughly described in [6] and [13] and subsequently extended to nonholonomic systems in [16]. The generalized-α integration scheme was used in [16]; this integrator is replaced here with the Newmark formulas [36] to obtain a simpler version of the algorithm.

Let us consider a multibody system modeled in terms of a set of parameters, $\boldsymbol{\rho} \in \mathbb{R}^p$, with $\mathbf{q}(\boldsymbol{\rho}, t) \in \mathbb{R}^{n_c}$ dependent coordinates related by m holonomic

$$\boldsymbol{\Phi}(\mathbf{q}, \boldsymbol{\rho}, t) = \mathbf{0} \tag{1}$$

and $\check{m}$ nonholonomic constraints

$$\check{\boldsymbol{\Phi}}(\mathbf{q}, \dot{\mathbf{q}}, \boldsymbol{\rho}, t) = \mathbf{A}(\mathbf{q}, \boldsymbol{\rho}, t)\,\dot{\mathbf{q}} + \mathbf{b}(\mathbf{q}, \boldsymbol{\rho}, t) = \mathbf{0} \tag{2}$$

Eq. (2) is expressed at the velocity level and, given the nonholonomic nature of these constraints, no configuration-level equivalent expression exists for it. Eq. (1) can be differentiated with respect to time to obtain the velocity-level expression of the holonomic constraints

$$\dot{\boldsymbol{\Phi}}(\mathbf{q}, \dot{\mathbf{q}}, \boldsymbol{\rho}, t) = \boldsymbol{\Phi}_{\mathbf{q}}\dot{\mathbf{q}} + \boldsymbol{\Phi}_t = \mathbf{0} \tag{3}$$

where $\boldsymbol{\Phi}_{\mathbf{q}} \equiv \partial\boldsymbol{\Phi}/\partial\mathbf{q} \in \mathbb{R}^{m \times n_c}$ is the Jacobian matrix of the holonomic constraints, and $\boldsymbol{\Phi}_t \equiv \partial\boldsymbol{\Phi}/\partial t$. Differentiation of Eqs. (3) and (2) with respect to time yields the acceleration-level

constraint equations

$$\ddot{\boldsymbol{\Phi}}\left(\mathbf{q},\dot{\mathbf{q}},\ddot{\mathbf{q}},\boldsymbol{\rho},t\right)=\boldsymbol{\Phi}_{\mathbf{q}}\ddot{\mathbf{q}}+\dot{\boldsymbol{\Phi}}_{\mathbf{q}}\dot{\mathbf{q}}+\dot{\boldsymbol{\Phi}}_{t}=\mathbf{0} \tag{4}$$

$$\dddot{\boldsymbol{\Phi}}\left(\mathbf{q},\dot{\mathbf{q}},\ddot{\mathbf{q}},\boldsymbol{\rho},t\right)=\mathbf{A}\ddot{\mathbf{q}}+\dot{\mathbf{A}}\dot{\mathbf{q}}+\dot{\mathbf{b}}=\mathbf{0} \tag{5}$$

The ALI3-P algorithm solves the system dynamics through an iterative algorithm in which only the configuration-level constraints $\boldsymbol{\Phi}=\mathbf{0}$ are enforced. Simplifying the generalized-α ALI3-P equations formulated in [16], the dynamic equilibrium at a single time step, t_{n+1}, can be established as

$$\left[\mathbf{M}\ddot{\mathbf{q}}+\boldsymbol{\Phi}_{\mathbf{q}}^{\mathrm{T}}\boldsymbol{\lambda}^{*(i+1)}+\boldsymbol{\Phi}_{\mathbf{q}}^{\mathrm{T}}\boldsymbol{\alpha}\boldsymbol{\Phi}\right]_{n+1}=\mathbf{Q}_{n+1} \tag{6a}$$

$$\boldsymbol{\lambda}_{n+1}^{*(i+1)}=\boldsymbol{\lambda}_{n+1}^{*(i)}+\boldsymbol{\alpha}\boldsymbol{\Phi}_{n+1}^{(i+1)};\quad i>0. \tag{6b}$$

where $\mathbf{M}\left(\mathbf{q},\boldsymbol{\rho}\right)\in\mathbb{R}^{n_c\times n_c}$ is the system mass matrix, term $\mathbf{Q}\left(\mathbf{q},\dot{\mathbf{q}},\boldsymbol{\rho}\right)\in\mathbb{R}^{n_c}$ represents the generalized applied forces and $\boldsymbol{\lambda}^{*}\left(\boldsymbol{\rho},t\right)\in\mathbb{R}^{m}$ are approximate Lagrange multipliers, evaluated iteratively and converging to the exact solution of the original index-3 DAE system, $\boldsymbol{\lambda}$, when $i\rightarrow\infty$. The Lagrange multipliers of the previous integration time-step are usually taken to start the iterative process in Eq. (6b), $\boldsymbol{\lambda}_{n+1}^{*(1)}=\boldsymbol{\lambda}_{n}^{*}$. Term $\boldsymbol{\alpha}\in\mathbb{R}^{m\times m}$ contains the penalty factors associated with the holonomic constraints; an interpretation of its physical meaning was provided in [30].

The dynamics equations (6) are usually combined with the integrator expressions, adopting the generalized coordinates $\mathbf{q}$ as primary variables, and solved through a Newton-Raphson iterative procedure. The Newmark method formulas are

$$\dot{\mathbf{q}}_{n+1}=\frac{\gamma}{\beta h}\mathbf{q}_{n+1}+\widehat{\dot{\mathbf{q}}}_{n};\quad\text{where }\widehat{\dot{\mathbf{q}}}_{n}=-\frac{\gamma}{\beta h}\mathbf{q}_{n}-\left(\frac{\gamma}{\beta}-1\right)\dot{\mathbf{q}}_{n}-h\left(\frac{\gamma}{2\beta}-1\right)\ddot{\mathbf{q}}_{n} \tag{7a}$$

$$\ddot{\mathbf{q}}_{n+1}=\frac{1}{\beta h^{2}}\mathbf{q}_{n+1}+\widehat{\ddot{\mathbf{q}}}_{n};\quad\text{where }\widehat{\ddot{\mathbf{q}}}_{n}=-\frac{1}{\beta h^{2}}\mathbf{q}_{n}-\frac{1}{\beta h}\dot{\mathbf{q}}_{n}-\left(\frac{1}{2\beta}-1\right)\ddot{\mathbf{q}}_{n} \tag{7b}$$

where h stands for the integration step-size and β and γ are scalar parameters of the integrator; subscript n denotes the time step. If $\beta=0.25$ and $\gamma=0.5$, Eqs. (7) become the well-known implicit trapezoidal rule method. The integrator equations (7) are introduced in the equations of motion (6a) and the dynamic equilibrium established at time t_{n+1} to formulate the dynamics

as the following system of nonlinear equations

$$[\mathbf{f}\ (\mathbf{q}_{n+1}, \boldsymbol{\rho})]^{(i)} = \mathbf{0} = \beta h^2 \mathbf{M} \widehat{\ddot{\mathbf{q}}}_n + \left[\mathbf{M}\mathbf{q} + \beta h^2 \boldsymbol{\Phi}_{\mathbf{q}}^{\mathrm{T}} \left(\boldsymbol{\lambda}^{*(i+1)} + \boldsymbol{\alpha}\boldsymbol{\Phi}\right) - \beta h^2 \mathbf{Q}\right]_{n+1} \tag{8}$$

with $\boldsymbol{\lambda}_{n+1}^{*(i+1)}$ given by Eq. (6b).

In each iteration i of the solution process the generalized coordinates, $\mathbf{q}_{n+1}^{(i)}$, are updated with an increment $\Delta\mathbf{q}^{(i+1)}$, evaluated as

$$\left[\frac{\partial \mathbf{f}\left(\mathbf{q}_{n+1}, \boldsymbol{\rho}\right)}{\partial \mathbf{q}_{n+1}}\right]^{(i)} \Delta\mathbf{q}^{(i+1)} = -\left[\mathbf{f}\left(\mathbf{q}_{n+1}, \boldsymbol{\rho}\right)\right]^{(i)} \tag{9}$$

with the approximate tangent matrix

$$\left[\frac{\partial \mathbf{f}\left(\mathbf{q}_{n+1}, \boldsymbol{\rho}\right)}{\partial \mathbf{q}_{n+1}}\right] = \mathbf{M} + \gamma h \mathbf{C} + \beta h^2 \left(\boldsymbol{\Phi}_{\mathbf{q}}^{\mathrm{T}} \boldsymbol{\alpha} \boldsymbol{\Phi}_{\mathbf{q}} + \mathbf{K}\right) \tag{10}$$

where $\mathbf{K} = -\mathbf{Q}_{\mathbf{q}} = -\partial\mathbf{Q}/\partial\mathbf{q}$ and $\mathbf{C} = -\mathbf{Q}_{\dot{\mathbf{q}}} = -\partial\mathbf{Q}/\partial\dot{\mathbf{q}}$. It was suggested in [13] that the approximate Lagrange multipliers $\boldsymbol{\lambda}^*$ are also updated during this iterative process with Eq. (6b). Upon convergence, the generalized coordinates at time-step $n+1$, $\mathbf{q}_{n+1}$ are obtained. The integrator expressions (7) then yield the approximate sets of generalized velocities and accelerations $\dot{\mathbf{q}}_{n+1}^*$ and $\ddot{\mathbf{q}}_{n+1}^*$.

It must be stressed that, as a configuration-level expression does not exist for nonholonomic constraints, the algorithm in Eqs. (6)–(10) does not enforce the kinematic relations in Eq. (2). Actually, the velocities $\dot{\mathbf{q}}_{n+1}^*$ and accelerations $\ddot{\mathbf{q}}_{n+1}^*$ obtained upon convergence of the algorithm do not satisfy exactly the velocity- and acceleration-level expressions of the holonomic constraints (3) and (4) either. These velocity- and acceleration-level expressions must be satisfied through the projection of the generalized velocities and accelerations onto their respective constraints manifolds. The correction introduced by the projections is usually small in the case of holonomic constraints, because their configuration-level expression has been satisfied as a result of the convergence of the Newton-Raphson iteration. In the case of nonholonomic constraints, however, the whole contribution of the constraint to the dynamics is imposed by the projections.

2.1 Velocity and acceleration projections

The velocity and acceleration projections arise as the solution of a minimization process [16] that consists on finding the velocities $\dot{\mathbf{q}}$ and accelerations $\ddot{\mathbf{q}}$ which are closest, in the sense of a norm defined by the selected projection matrix, to the ones delivered by the Newton-Raphson iteration, $\dot{\mathbf{q}}^*_{n+1}$ and $\ddot{\mathbf{q}}^*_{n+1}$, while fulfilling the kinematic constraints in Eqs. (2)–(5). For the sake of clarity, both the holonomic and the nonholonomic constraints in Eqs. (2) and (3) will be treated together at this stage of the algorithm, grouping the velocity-level constraints in term

$$\bar{\boldsymbol{\Phi}}\left(\mathbf{q},\dot{\mathbf{q}},\boldsymbol{\rho},t\right)=\begin{bmatrix}\dot{\boldsymbol{\Phi}}\\ \check{\boldsymbol{\Phi}}\end{bmatrix}=\bar{\mathbf{A}}\dot{\mathbf{q}}+\bar{\mathbf{b}}=\mathbf{0} \tag{11}$$

where

$$\bar{\mathbf{A}}=\begin{bmatrix}\boldsymbol{\Phi}_{\mathbf{q}}\\ \mathbf{A}\end{bmatrix};\qquad \bar{\mathbf{b}}=\begin{bmatrix}\boldsymbol{\Phi}_{t}\\ \mathbf{b}\end{bmatrix} \tag{12}$$

The total number of velocity-level constraints is $\bar{m}=m+\check{m}$.

The projection of velocities is carried out with the iterative algorithm

$$\left(\mathbf{P}+\varsigma\bar{\mathbf{A}}^{\mathrm{T}}\bar{\boldsymbol{\alpha}}\bar{\mathbf{A}}\right)\dot{\mathbf{q}}^{(i+1)}=\mathbf{P}\dot{\mathbf{q}}^{*}-\varsigma\bar{\mathbf{A}}^{\mathrm{T}}\bar{\boldsymbol{\alpha}}\bar{\mathbf{b}}-\bar{\mathbf{A}}^{\mathrm{T}}\bar{\boldsymbol{\sigma}}^{(i+1)} \tag{13a}$$

$$\bar{\boldsymbol{\sigma}}^{(i+1)}=\bar{\boldsymbol{\sigma}}^{(i)}+\varsigma\bar{\boldsymbol{\alpha}}\bar{\boldsymbol{\Phi}} \tag{13b}$$

where $\mathbf{P}$ is the $n\times n$ projection matrix, $\bar{\boldsymbol{\sigma}}$ contains the $\bar{m}$ Lagrange multipliers of the minimization problem associated with the velocity projection; ς is a scalar weighting constant and $\bar{\boldsymbol{\alpha}}\in\mathbb{R}^{\bar{m}\times\bar{m}}$ is a penalty matrix that now includes the penalty factors for the holonomic and nonholonomic constraint equations, $\check{\boldsymbol{\alpha}}\in\mathbb{R}^{\check{m}\times\check{m}}$, as well

$$\bar{\boldsymbol{\alpha}}=\begin{bmatrix}\boldsymbol{\alpha} & \mathbf{0}_{m\times\check{m}}\\ \mathbf{0}_{\check{m}\times m} & \check{\boldsymbol{\alpha}}\end{bmatrix} \tag{14}$$

Similar equations are used to project the accelerations

$$\left(\mathbf{P} + \varsigma \bar{\mathbf{A}}^{\mathrm{T}} \bar{\boldsymbol{\alpha}} \bar{\mathbf{A}}\right) \ddot{\mathbf{q}}^{(i+1)} = \mathbf{P} \ddot{\mathbf{q}}^{*} - \varsigma \bar{\mathbf{A}}^{\mathrm{T}} \bar{\boldsymbol{\alpha}} \left(\dot{\bar{\mathbf{A}}} \dot{\mathbf{q}} + \dot{\bar{\mathbf{b}}}\right) - \bar{\mathbf{A}}^{\mathrm{T}} \bar{\boldsymbol{\kappa}}^{(i+1)} \tag{15a}$$

$$\bar{\boldsymbol{\kappa}}^{(i+1)} = \bar{\boldsymbol{\kappa}}^{(i)} + \varsigma \bar{\boldsymbol{\alpha}} \dot{\bar{\boldsymbol{\Phi}}} \tag{15b}$$

where $\bar{\boldsymbol{\kappa}}$ are the Lagrange multipliers of the acceleration minimization problem and $\dot{\bar{\boldsymbol{\Phi}}}$ is a vector containing both the holonomic, $\ddot{\boldsymbol{\Phi}}$, and nonholonomic, $\dot{\bar{\boldsymbol{\Phi}}}$, constraints at acceleration level,

$$\dot{\bar{\boldsymbol{\Phi}}} = \begin{bmatrix} \ddot{\boldsymbol{\Phi}} \\ \dot{\bar{\boldsymbol{\Phi}}} \end{bmatrix} = \bar{\mathbf{A}} \ddot{\mathbf{q}} + \dot{\bar{\mathbf{A}}} \dot{\mathbf{q}} + \dot{\bar{\mathbf{b}}} = \mathbf{0} \tag{16}$$

Several options exist for the selection of the projection matrix $\mathbf{P}$ and the weighting constant ς. A possibility is using the mass-orthogonal projections in [6]. In this case

$$\mathbf{P} = \mathbf{M} \tag{17a}$$

$$\varsigma = 1 \tag{17b}$$

The mass-stiffness-damping-orthogonal projections in [13] are also frequently found in multibody applications. The extension of these to the nonholonomic case yields the following expressions [16]

$$\mathbf{P} = \mathbf{M} + \gamma h \mathbf{C} + \beta h^2 \mathbf{K} - \varsigma \mathbf{A}^{\mathrm{T}} \check{\boldsymbol{\alpha}} \mathbf{A} \tag{18a}$$

$$\varsigma = \beta h^2 \tag{18b}$$

3 Sensitivity analysis of the ALI3-P formulation

Let $\boldsymbol{\psi} \in \mathbb{R}^o$ be a collection of o objective functions defined in terms of the parameters $\boldsymbol{\rho}$, the generalized coordinates and their derivatives $\mathbf{q}$, $\dot{\mathbf{q}}$, $\ddot{\mathbf{q}}$, the Lagrange multipliers of the dynamics $\boldsymbol{\lambda}^*$ and, possibly, the Lagrange multipliers of the projections, $\bar{\boldsymbol{\sigma}}$ and $\bar{\boldsymbol{\kappa}}$. If t_0 and t_F are the starting and final time of the system motion, then the objective functions can be expressed as the sum of

a term that depends on the final state of the system and an integral from t_0 to t_F.

$$\boldsymbol{\psi} = \mathbf{w}\left(\mathbf{q}, \dot{\mathbf{q}}, \ddot{\mathbf{q}}, \boldsymbol{\lambda}^*, \bar{\boldsymbol{\sigma}}, \bar{\boldsymbol{\kappa}}, \boldsymbol{\rho}\right)_F + \int_{t_0}^{t_F} \mathbf{g}\left(\mathbf{q}, \dot{\mathbf{q}}, \ddot{\mathbf{q}}, \boldsymbol{\lambda}^*, \bar{\boldsymbol{\sigma}}, \bar{\boldsymbol{\kappa}}, \boldsymbol{\rho}\right) \mathrm{d}t \tag{19}$$

where $\mathbf{w} \in \mathbb{R}^o$ and $\mathbf{g} \in \mathbb{R}^o$ are column vectors of o scalar functions of the variables and the subscript F stands for evaluation at time t_F. The sensitivity of the cost functions is expressed by the gradient

$$\begin{aligned} \nabla_{\boldsymbol{\rho}} \boldsymbol{\psi}^{\mathrm{T}} = \frac{\partial \boldsymbol{\psi}}{\partial \boldsymbol{\rho}} = & \left(\mathbf{w}_{\mathbf{q}}\mathbf{q}_{\boldsymbol{\rho}} + \mathbf{w}_{\dot{\mathbf{q}}}\dot{\mathbf{q}}_{\boldsymbol{\rho}} + \mathbf{w}_{\ddot{\mathbf{q}}}\ddot{\mathbf{q}}_{\boldsymbol{\rho}} + \mathbf{w}_{\boldsymbol{\lambda}^*}\boldsymbol{\lambda}^*_{\boldsymbol{\rho}} + \mathbf{w}_{\bar{\boldsymbol{\sigma}}}\bar{\boldsymbol{\sigma}}_{\boldsymbol{\rho}} + \mathbf{w}_{\bar{\boldsymbol{\kappa}}}\bar{\boldsymbol{\kappa}}_{\boldsymbol{\rho}} + \mathbf{w}_{\boldsymbol{\rho}}\right)_F \\ & + \int_{t_0}^{t_F} \left(g_{\mathbf{q}}\mathbf{q}_{\boldsymbol{\rho}} + g_{\dot{\mathbf{q}}}\dot{\mathbf{q}}_{\boldsymbol{\rho}} + g_{\ddot{\mathbf{q}}}\ddot{\mathbf{q}}_{\boldsymbol{\rho}} + g_{\boldsymbol{\lambda}^*}\boldsymbol{\lambda}^*_{\boldsymbol{\rho}} + g_{\bar{\boldsymbol{\sigma}}}\bar{\boldsymbol{\sigma}}_{\boldsymbol{\rho}} + g_{\bar{\boldsymbol{\kappa}}}\bar{\boldsymbol{\kappa}}_{\boldsymbol{\rho}} + g_{\boldsymbol{\rho}}\right) \mathrm{d}t \end{aligned} \tag{20}$$

where the subscripts stand for derivatives. In Eq. (20) the derivatives of functions $\mathbf{w}$ and $\mathbf{g}$ are known, since the objective function has a known expression. This is not the case of magnitudes $\mathbf{q}_{\boldsymbol{\rho}}$, $\dot{\mathbf{q}}_{\boldsymbol{\rho}}$, $\ddot{\mathbf{q}}_{\boldsymbol{\rho}} \in \mathbb{R}^{n_c \times p}$, $\boldsymbol{\lambda}^*_{\boldsymbol{\rho}} \in \mathbb{R}^{m \times p}$, and $\bar{\boldsymbol{\sigma}}_{\boldsymbol{\rho}}$, $\bar{\boldsymbol{\kappa}}_{\boldsymbol{\rho}} \in \mathbb{R}^{\bar{m} \times p}$. These are the sensitivity matrices solution of a set of p DAE systems called the Tangent Linear Model (TLM) of the equations of motion, plus p velocity and p acceleration sensitivity projections.

The TLM of the dynamics equations can be obtained differentiating Eq. (6) with respect of each one of the p system parameters

$$\frac{\mathrm{d}\mathbf{M}}{\mathrm{d}\rho_k}\ddot{\mathbf{q}} + \mathbf{M}\frac{\mathrm{d}\ddot{\mathbf{q}}}{\mathrm{d}\rho_k} + \frac{\mathrm{d}\boldsymbol{\Phi}_{\mathbf{q}}^{\mathrm{T}}}{\mathrm{d}\rho_k}\left(\boldsymbol{\lambda}^* + \boldsymbol{\alpha}\boldsymbol{\Phi}\right) + \boldsymbol{\Phi}_{\mathbf{q}}^{\mathrm{T}}\left(\frac{\mathrm{d}\boldsymbol{\lambda}^{*(i+1)}}{\mathrm{d}\rho_k} + \boldsymbol{\alpha}\frac{\mathrm{d}\boldsymbol{\Phi}}{\mathrm{d}\rho_k}\right) = \frac{\mathrm{d}\mathbf{Q}}{\mathrm{d}\rho_k}\,; \tag{21a}$$

$$\frac{\mathrm{d}\boldsymbol{\lambda}^{*(i+1)}}{\mathrm{d}\rho_k} = \frac{\mathrm{d}\boldsymbol{\lambda}^{*(i)}}{\mathrm{d}\rho_k} + \boldsymbol{\alpha}\frac{\mathrm{d}\boldsymbol{\Phi}}{\mathrm{d}\rho_k}, \quad i > 0;\ k = 1, \ldots, p \tag{21b}$$

and following the same strategy employed for the dynamics, the iteration of the sensitivities of the Lagrange multipliers has to be started as

$$\frac{\mathrm{d}\boldsymbol{\lambda}^{*(1)}_{n+1}}{\mathrm{d}\rho_k} = \frac{\mathrm{d}\boldsymbol{\lambda}^*_n}{\mathrm{d}\rho_k} \tag{22}$$

The differentiation of the velocity projections (13) with respect to the parameters $\boldsymbol{\rho}$ yields

$$\begin{aligned}\left[\frac{\mathrm{d}\mathbf{P}}{\mathrm{d}\rho_k}+\varsigma\left(\frac{\mathrm{d}\bar{\mathbf{A}}^{\mathrm{T}}}{\mathrm{d}\rho_k}\bar{\boldsymbol{\alpha}}\bar{\mathbf{A}}+\bar{\mathbf{A}}^{\mathrm{T}}\bar{\boldsymbol{\alpha}}\frac{\mathrm{d}\bar{\mathbf{A}}}{\mathrm{d}\rho_k}\right)\right]\dot{\mathbf{q}}+\left(\mathbf{P}+\varsigma\bar{\mathbf{A}}^{\mathrm{T}}\bar{\boldsymbol{\alpha}}\bar{\mathbf{A}}\right)\frac{\mathrm{d}\dot{\mathbf{q}}^{(i+1)}}{\mathrm{d}\rho_k}\\ =\frac{\mathrm{d}\mathbf{P}}{\mathrm{d}\rho_k}\dot{\mathbf{q}}^{*}+\mathbf{P}\frac{\mathrm{d}\dot{\mathbf{q}}^{*}}{\mathrm{d}\rho_k}-\frac{\mathrm{d}\bar{\mathbf{A}}^{\mathrm{T}}}{\mathrm{d}\rho_k}\left(\bar{\boldsymbol{\sigma}}+\varsigma\bar{\boldsymbol{\alpha}}\bar{\mathbf{b}}\right)-\bar{\mathbf{A}}^{\mathrm{T}}\left(\frac{\mathrm{d}\bar{\boldsymbol{\sigma}}^{(i+1)}}{\mathrm{d}\rho_k}+\varsigma\bar{\boldsymbol{\alpha}}\frac{\mathrm{d}\bar{\mathbf{b}}}{\mathrm{d}\rho_k}\right)\end{aligned} \tag{23a}$$

$$\frac{\mathrm{d}\bar{\boldsymbol{\sigma}}^{(i+1)}}{\mathrm{d}\rho_k}=\frac{\mathrm{d}\bar{\boldsymbol{\sigma}}^{(i)}}{\mathrm{d}\rho_k}+\varsigma\bar{\boldsymbol{\alpha}}\frac{\mathrm{d}\bar{\boldsymbol{\Phi}}}{\mathrm{d}\rho_k} \tag{23b}$$

Similarly, differentiating the acceleration projections (15) one obtains

$$\begin{aligned}\left[\frac{\mathrm{d}\mathbf{P}}{\mathrm{d}\rho_k}+\varsigma\left(\frac{\mathrm{d}\bar{\mathbf{A}}^{\mathrm{T}}}{\mathrm{d}\rho_k}\bar{\boldsymbol{\alpha}}\bar{\mathbf{A}}+\bar{\mathbf{A}}^{\mathrm{T}}\bar{\boldsymbol{\alpha}}\frac{\mathrm{d}\bar{\mathbf{A}}}{\mathrm{d}\rho_k}\right)\right]\ddot{\mathbf{q}}+\left(\mathbf{P}+\varsigma\bar{\mathbf{A}}^{\mathrm{T}}\bar{\boldsymbol{\alpha}}\bar{\mathbf{A}}\right)\frac{\mathrm{d}\ddot{\mathbf{q}}^{(i+1)}}{\mathrm{d}\rho_k}\\ =\frac{\mathrm{d}\mathbf{P}}{\mathrm{d}\rho_k}\ddot{\mathbf{q}}^{*}+\mathbf{P}\frac{\mathrm{d}\ddot{\mathbf{q}}^{*}}{\mathrm{d}\rho_k}-\frac{\mathrm{d}\bar{\mathbf{A}}^{\mathrm{T}}}{\mathrm{d}\rho_k}\left[\bar{\boldsymbol{\kappa}}+\varsigma\bar{\boldsymbol{\alpha}}\left(\dot{\bar{\mathbf{A}}}\dot{\mathbf{q}}+\dot{\bar{\mathbf{b}}}\right)\right]\\ -\bar{\mathbf{A}}^{\mathrm{T}}\left[\frac{\mathrm{d}\bar{\boldsymbol{\kappa}}^{(k+1)}}{\mathrm{d}\rho_k}+\varsigma\bar{\boldsymbol{\alpha}}\left(\frac{\mathrm{d}\dot{\bar{\mathbf{A}}}\dot{\mathbf{q}}}{\mathrm{d}\rho_k}+\frac{\mathrm{d}\dot{\bar{\mathbf{b}}}}{\mathrm{d}\rho_k}\right)\right]\end{aligned} \tag{24a}$$

$$\frac{\mathrm{d}\bar{\boldsymbol{\kappa}}^{(i+1)}}{\mathrm{d}\rho_k}=\frac{\mathrm{d}\bar{\boldsymbol{\kappa}}^{(i)}}{\mathrm{d}\rho_k}+\varsigma\bar{\boldsymbol{\alpha}}\frac{\mathrm{d}\dot{\bar{\boldsymbol{\Phi}}}}{\mathrm{d}\rho_k} \tag{24b}$$

Expanding the total derivatives and grouping them together in tensor-matrix notation leads to the following set of p DAEs for the TLM of the dynamics in Eq. (21)

$$\begin{aligned}\left(\mathbf{M}_{\mathbf{q}}\ddot{\mathbf{q}}^{*}+\boldsymbol{\Phi}_{\mathbf{qq}}^{\mathrm{T}}\left(\boldsymbol{\lambda}^{*}+\boldsymbol{\alpha}\boldsymbol{\Phi}\right)+\boldsymbol{\Phi}_{\mathbf{q}}^{\mathrm{T}}\boldsymbol{\alpha}\boldsymbol{\Phi}_{\mathbf{q}}+\mathbf{K}\right)\mathbf{q}_{\boldsymbol{\rho}}+\mathbf{M}\ddot{\mathbf{q}}_{\boldsymbol{\rho}}^{*}+\mathbf{C}\dot{\mathbf{q}}_{\boldsymbol{\rho}}^{*}+\boldsymbol{\Phi}_{\mathbf{q}}^{\mathrm{T}}\boldsymbol{\lambda}_{\boldsymbol{\rho}}^{*(i+1)}\\ =\mathbf{Q}_{\boldsymbol{\rho}}-\mathbf{M}_{\boldsymbol{\rho}}\ddot{\mathbf{q}}^{*}-\boldsymbol{\Phi}_{\mathbf{q}\boldsymbol{\rho}}^{\mathrm{T}}\left(\boldsymbol{\lambda}^{*}+\boldsymbol{\alpha}\boldsymbol{\Phi}\right)-\boldsymbol{\Phi}_{\mathbf{q}}^{\mathrm{T}}\boldsymbol{\alpha}\boldsymbol{\Phi}_{\boldsymbol{\rho}}\end{aligned} \tag{25a}$$

$$\boldsymbol{\lambda}_{\boldsymbol{\rho}}^{*(i+1)}=\boldsymbol{\lambda}_{\boldsymbol{\rho}}^{*(i)}+\boldsymbol{\alpha}\left(\boldsymbol{\Phi}_{\mathbf{q}}\mathbf{q}_{\boldsymbol{\rho}}+\boldsymbol{\Phi}_{\boldsymbol{\rho}}\right) \tag{25b}$$

where the following terms are tensor-vector products: $\mathbf{M}_{\mathbf{q}}\ddot{\mathbf{q}}\equiv\mathbf{M}_{\mathbf{q}}\otimes\ddot{\mathbf{q}}$, $\boldsymbol{\Phi}_{\mathbf{qq}}^{\mathrm{T}}\left(\boldsymbol{\lambda}^{*}+\boldsymbol{\alpha}\boldsymbol{\Phi}\right)\equiv\boldsymbol{\Phi}_{\mathbf{qq}}^{\mathrm{T}}\otimes\left(\boldsymbol{\lambda}^{*}+\boldsymbol{\alpha}\boldsymbol{\Phi}\right)$, $\mathbf{M}_{\boldsymbol{\rho}}\ddot{\mathbf{q}}\equiv\mathbf{M}_{\boldsymbol{\rho}}\otimes\ddot{\mathbf{q}}$, $\boldsymbol{\Phi}_{\mathbf{q}\boldsymbol{\rho}}^{\mathrm{T}}\left(\boldsymbol{\lambda}^{*}+\boldsymbol{\alpha}\boldsymbol{\Phi}\right)\equiv\boldsymbol{\Phi}_{\mathbf{q}\boldsymbol{\rho}}^{\mathrm{T}}\otimes\left(\boldsymbol{\lambda}^{*}+\boldsymbol{\alpha}\boldsymbol{\Phi}\right)$.

The corresponding system of equations for the sensitivity of the projected velocities (23) is

$$\begin{aligned}\left(\mathbf{P}+\varsigma\bar{\mathbf{A}}^{\mathrm{T}}\bar{\boldsymbol{\alpha}}\bar{\mathbf{A}}\right)\dot{\mathbf{q}}_{\boldsymbol{\rho}}^{(i+1)}=\mathbf{P}\dot{\mathbf{q}}_{\boldsymbol{\rho}}^{*}+\frac{\mathrm{d}\mathbf{P}}{\mathrm{d}\boldsymbol{\rho}}\left(\dot{\mathbf{q}}^{*}-\dot{\mathbf{q}}\right)\\ -\bar{\mathbf{A}}_{\mathbf{q}}^{\mathrm{T}}\left(\bar{\boldsymbol{\sigma}}+\varsigma\bar{\boldsymbol{\alpha}}\bar{\boldsymbol{\Phi}}\right)\mathbf{q}_{\boldsymbol{\rho}}-\bar{\mathbf{A}}_{\boldsymbol{\rho}}^{\mathrm{T}}\left(\bar{\boldsymbol{\sigma}}+\varsigma\bar{\boldsymbol{\alpha}}\bar{\boldsymbol{\Phi}}\right)-\bar{\mathbf{A}}^{\mathrm{T}}\left(\bar{\boldsymbol{\sigma}}_{\boldsymbol{\rho}}^{(i+1)}+\varsigma\bar{\boldsymbol{\alpha}}\mathbf{b}^{\boldsymbol{\rho}}\right)\end{aligned} \tag{26a}$$

$$\bar{\boldsymbol{\sigma}}_{\boldsymbol{\rho}}^{(i+1)}=\bar{\boldsymbol{\sigma}}_{\boldsymbol{\rho}}^{(i)}+\varsigma\bar{\boldsymbol{\alpha}}\frac{\mathrm{d}\bar{\boldsymbol{\Phi}}}{\mathrm{d}\boldsymbol{\rho}} \tag{26b}$$

and the system for the projected accelerations (24) takes the form

$$\begin{aligned}\left(\mathbf{P}+\varsigma\bar{\mathbf{A}}^{\mathrm{T}}\bar{\boldsymbol{\alpha}}\bar{\mathbf{A}}\right)\ddot{\mathbf{q}}_{\boldsymbol{\rho}}^{(i+1)} &= \mathbf{P}\ddot{\mathbf{q}}_{\boldsymbol{\rho}}^{*}+\frac{\mathrm{d}\mathbf{P}}{\mathrm{d}\boldsymbol{\rho}}\left(\ddot{\mathbf{q}}^{*}-\ddot{\mathbf{q}}\right)\\ &-\bar{\mathbf{A}}_{\mathbf{q}}^{\mathrm{T}}\left(\bar{\boldsymbol{\kappa}}+\varsigma\bar{\boldsymbol{\alpha}}\dot{\bar{\boldsymbol{\Phi}}}\right)\mathbf{q}_{\boldsymbol{\rho}}-\bar{\mathbf{A}}_{\boldsymbol{\rho}}^{\mathrm{T}}\left(\bar{\boldsymbol{\kappa}}+\varsigma\bar{\boldsymbol{\alpha}}\dot{\bar{\boldsymbol{\Phi}}}\right)-\bar{\mathbf{A}}^{\mathrm{T}}\left(\bar{\boldsymbol{\kappa}}_{\boldsymbol{\rho}}^{(i+1)}+\varsigma\bar{\boldsymbol{\alpha}}\mathbf{c}^{\boldsymbol{\rho}}\right)\end{aligned} \tag{27a}$$

$$\bar{\boldsymbol{\kappa}}_{\boldsymbol{\rho}}^{(i+1)}=\bar{\boldsymbol{\kappa}}_{\boldsymbol{\rho}}^{(i)}+\varsigma\bar{\boldsymbol{\alpha}}\frac{\mathrm{d}\dot{\bar{\boldsymbol{\Phi}}}}{\mathrm{d}\boldsymbol{\rho}} \tag{27b}$$

where

$$\frac{\mathrm{d}\bar{\boldsymbol{\Phi}}}{\mathrm{d}\boldsymbol{\rho}}=\bar{\mathbf{A}}\dot{\mathbf{q}}_{\boldsymbol{\rho}}+\mathbf{b}^{\boldsymbol{\rho}} \tag{28}$$

$$\frac{\mathrm{d}\dot{\bar{\boldsymbol{\Phi}}}}{\mathrm{d}\boldsymbol{\rho}}=\bar{\mathbf{A}}\ddot{\mathbf{q}}_{\boldsymbol{\rho}}+\mathbf{c}^{\boldsymbol{\rho}} \tag{29}$$

$$\mathbf{b}^{\boldsymbol{\rho}}=\left(\bar{\mathbf{A}}_{\mathbf{q}}\dot{\mathbf{q}}+\bar{\mathbf{b}}_{\mathbf{q}}\right)\mathbf{q}_{\boldsymbol{\rho}}+\bar{\mathbf{A}}_{\boldsymbol{\rho}}\dot{\mathbf{q}}+\bar{\mathbf{b}}_{\boldsymbol{\rho}}=\dot{\bar{\mathbf{A}}}\mathbf{q}_{\boldsymbol{\rho}}+\bar{\boldsymbol{\Phi}}_{\boldsymbol{\rho}} \tag{30}$$

$$\begin{aligned}\mathbf{c}^{\boldsymbol{\rho}} &= \left(\bar{\mathbf{A}}_{\mathbf{q}}\dot{\mathbf{q}}+\dot{\bar{\mathbf{A}}}+\bar{\mathbf{b}}_{\mathbf{q}}\right)\dot{\mathbf{q}}_{\boldsymbol{\rho}}+\left(\bar{\mathbf{A}}_{\mathbf{q}}\ddot{\mathbf{q}}+\dot{\bar{\mathbf{A}}}_{\mathbf{q}}\dot{\mathbf{q}}+\dot{\bar{\mathbf{b}}}_{\mathbf{q}}\right)\mathbf{q}_{\boldsymbol{\rho}}\\ &+\bar{\mathbf{A}}_{\boldsymbol{\rho}}\ddot{\mathbf{q}}+\dot{\bar{\mathbf{A}}}_{\boldsymbol{\rho}}\dot{\mathbf{q}}+\dot{\bar{\mathbf{b}}}_{\boldsymbol{\rho}}=2\dot{\bar{\mathbf{A}}}\dot{\mathbf{q}}_{\boldsymbol{\rho}}+\dot{\bar{\boldsymbol{\Phi}}}_{\mathbf{q}}\mathbf{q}_{\boldsymbol{\rho}}+\dot{\bar{\boldsymbol{\Phi}}}_{\boldsymbol{\rho}}\end{aligned} \tag{31}$$

It must be noted that term $\mathrm{d}\mathbf{P}/\mathrm{d}\boldsymbol{\rho}$ depends on the selection of the projection matrix. For all the numerical experiments solved in this work, the mass-orthogonal projections, $\mathbf{P}=\mathbf{M}$, $\varsigma=1$ will be used.

3.1 Algorithm implementation

The evaluation of the numerical sensitivities of a mechanical system must take place after the system dynamics has been solved and integrated, using to this end the expression in Section 2. Once the dynamics is known, it is possible to proceed to the evaluation and integration of the system sensitivities.

The TLM in Eqs. (25) features four sets of unknowns, namely $\mathbf{q}_{\boldsymbol{\rho}}$, $\dot{\mathbf{q}}_{\boldsymbol{\rho}}^{*}$, $\ddot{\mathbf{q}}_{\boldsymbol{\rho}}^{*}$, and $\boldsymbol{\lambda}_{\boldsymbol{\rho}}^{*}$. This TLM requires $2n_cp$ initial conditions in the form

$$\mathbf{q}_{\boldsymbol{\rho}}\left(t_0\right)=\mathbf{q}_{\boldsymbol{\rho}0}\,;\qquad\dot{\mathbf{q}}_{\boldsymbol{\rho}}\left(t_0\right)=\dot{\mathbf{q}}_{\boldsymbol{\rho}0} \tag{32}$$

These initial conditions have to satisfy the following constraint equations

$$\frac{\mathrm{d}\boldsymbol{\Phi}\left(t_0\right)}{\mathrm{d}\boldsymbol{\rho}} = \mathbf{0} \rightarrow \left[\boldsymbol{\Phi}_{\mathbf{q}}\mathbf{q}_{\boldsymbol{\rho}}\right]_0 = -\boldsymbol{\Phi}_{\boldsymbol{\rho}0} \tag{33a}$$

$$\frac{\mathrm{d}\bar{\boldsymbol{\Phi}}\left(t_0\right)}{\mathrm{d}\boldsymbol{\rho}} = \mathbf{0} \rightarrow \left[\bar{\mathbf{A}}\dot{\mathbf{q}}_{\boldsymbol{\rho}}\right]_0 = -\left[\mathbf{b}^{\boldsymbol{\rho}}\right]_0 \tag{33b}$$

Eqs. (25) can be reduced to a nonlinear system of equations with the sensitivities $\mathbf{q}_{\boldsymbol{\rho}}$ and $\boldsymbol{\lambda}^*_{\boldsymbol{\rho}}$ as only unknowns introducing in Eq. (25a) the numerical integrator expressions.

If the Newmark integration scheme is used, then

$$\begin{aligned}
&\dot{\mathbf{q}}^*_{\boldsymbol{\rho},n+1} = \frac{\gamma}{\beta h}\mathbf{q}_{\boldsymbol{\rho},n+1} + \widehat{\dot{\mathbf{q}}}_{\boldsymbol{\rho},n}\,; \qquad \text{where} \\
&\widehat{\dot{\mathbf{q}}}_{\boldsymbol{\rho},n} = \frac{-\gamma}{\beta h}\mathbf{q}_{\boldsymbol{\rho},n} - \left(\frac{\gamma}{\beta} - 1\right)\dot{\mathbf{q}}_{\boldsymbol{\rho},n} - h\left(\frac{\gamma}{2\beta} - 1\right)\ddot{\mathbf{q}}_{\boldsymbol{\rho},n}
\end{aligned} \tag{34a}$$

$$\begin{aligned}
&\ddot{\mathbf{q}}^*_{\boldsymbol{\rho},n+1} = \frac{1}{\beta h^2}\mathbf{q}_{\boldsymbol{\rho},n+1} + \widehat{\ddot{\mathbf{q}}}_{\boldsymbol{\rho},n}\,; \qquad \text{where} \\
&\widehat{\ddot{\mathbf{q}}}_{\boldsymbol{\rho},n} = -\frac{1}{\beta h^2}\mathbf{q}_{\boldsymbol{\rho},n} - \frac{1}{\beta h}\dot{\mathbf{q}}_{\boldsymbol{\rho},n} - \left(\frac{1}{2\beta} - 1\right)\ddot{\mathbf{q}}_{\boldsymbol{\rho},n}
\end{aligned} \tag{34b}$$

Introducing Eqs. (34) in Eq. (25a), the TLM becomes, at time $t = t_{n+1}$,

$$\begin{aligned}
&\left[\mathbf{M} + \gamma h\mathbf{C} + \beta h^2\left(\mathbf{M}_{\mathbf{q}}\ddot{\mathbf{q}}^* + \boldsymbol{\Phi}^{\mathrm{T}}_{\mathbf{qq}}\left(\boldsymbol{\lambda}^* + \boldsymbol{\alpha}\boldsymbol{\Phi}\right) + \boldsymbol{\Phi}^{\mathrm{T}}_{\mathbf{q}}\boldsymbol{\alpha}\boldsymbol{\Phi}_{\mathbf{q}} + \mathbf{K}\right)\right]\mathbf{q}_{\boldsymbol{\rho}} \\
&\quad = \beta h^2\left(\mathbf{Q}_{\boldsymbol{\rho}} - \mathbf{M}_{\boldsymbol{\rho}}\ddot{\mathbf{q}}^* - \boldsymbol{\Phi}^{\mathrm{T}}_{\mathbf{q}\boldsymbol{\rho}}\left(\boldsymbol{\lambda}^* + \boldsymbol{\alpha}\boldsymbol{\Phi}\right) - \boldsymbol{\Phi}^{\mathrm{T}}_{\mathbf{q}}\boldsymbol{\alpha}\boldsymbol{\Phi}_{\boldsymbol{\rho}} - \boldsymbol{\Phi}^{\mathrm{T}}_{\mathbf{q}}\boldsymbol{\lambda}^*_{\boldsymbol{\rho}} - \mathbf{M}\widehat{\ddot{\mathbf{q}}}_{\boldsymbol{\rho},n} - \mathbf{C}\widehat{\dot{\mathbf{q}}}_{\boldsymbol{\rho},n}\right)
\end{aligned} \tag{35a}$$

$$\boldsymbol{\lambda}^{*(i+1)}_{\boldsymbol{\rho}} = \boldsymbol{\lambda}^{*(i)}_{\boldsymbol{\rho}} + \boldsymbol{\alpha}\left(\boldsymbol{\Phi}_{\mathbf{q}}\mathbf{q}_{\boldsymbol{\rho}} + \boldsymbol{\Phi}_{\boldsymbol{\rho}}\right) \tag{35b}$$

Note that both sides in Eq. (35a) were scaled with βh^2 to match the expression of the system dynamics in Eq. (8). Equation (35a) is a linear system of equations in $\mathbf{q}_{\boldsymbol{\rho}}$; even though, an iterative solution process is required to ensure the convergence of the sensitivities of the Lagrange multipliers, $\boldsymbol{\lambda}^*_{\boldsymbol{\rho}}$, which enter the right-hand side of Eq. (35a). Accordingly, this equation must be solved together with the iterative update provided in Eq. (35b). Upon convergence, the values of the sensitivities $\mathbf{q}_{\boldsymbol{\rho},n}$ and $\boldsymbol{\lambda}^*_{\boldsymbol{\rho},n}$ are known, and the approximate values of the sensitivities of the velocities and accelerations, $\dot{\mathbf{q}}^*_{\boldsymbol{\rho},n}$ and $\ddot{\mathbf{q}}^*_{\boldsymbol{\rho},n}$ can be obtained from the integrator equations, (34). Finally, the sensitivities of the projected velocities and accelerations, $\dot{\mathbf{q}}_{\boldsymbol{\rho},n}$ and $\ddot{\mathbf{q}}_{\boldsymbol{\rho},n}$ are obtained from the solution of the iterative processes in Eqs. (26)–(31). During this stage the sensitivities of the Lagrange multipliers of the projections, $\bar{\boldsymbol{\sigma}}_{\boldsymbol{\rho}}$ and $\bar{\boldsymbol{\kappa}}_{\boldsymbol{\rho}}$, are evaluated as well.

The evaluation of terms $\widehat{\dot{\mathbf{q}}}_{\boldsymbol{\rho},n}$ and $\widehat{\ddot{\mathbf{q}}}_{\boldsymbol{\rho},n}$ at time t_0 requires the availability of the initial sensitivities of the system accelerations, $\ddot{\mathbf{q}}_{\boldsymbol{\rho}0}$. Similarly, an initial value of the sensitivities of the Lagrange multipliers, $\boldsymbol{\lambda}^*_{\boldsymbol{\rho}0}$ is needed to start the iterative process in Eq. (25b). Both these terms can be provided at $t = t_0$ by means of an index-1 direct sensitivity algorithm, such as the penalty or the index-1 augmented Lagrangian (ALI1) formulations described in [19].

4 Numerical experiments

The formulation described in Section 3 was tested in the sensitivity analysis of three mechanical systems.

4.1 Five-bar mechanism

The first test problem is a two-degree-of-freedom five-bar linkage, shown in Fig. 1. The five bars are connected by revolute joints at points A, 1, 2, 3, and B. Points A and B are fixed to the ground. The masses of the rods are $m_{A1} = 1$ kg, $m_{12} = 1.5$ kg, $m_{23} = 1.5$ kg, and $m_{3B} = 1$ kg. The rotational moments of inertia are evaluated assuming an uniform mass distribution in each rod. The system moves under gravity effects, $g = 9.81$ m/s^2 along the negative vertical direction, and is subjected to the action of two linear springs with elastic constants $k_1 = k_2 = 100$ N/m. The natural lengths of these springs are the system parameters, $\boldsymbol{\rho} = [L_{01}, L_{02}]^{\mathrm{T}}$, and their initial values are selected to match the initial configuration shown in Fig. 1, $L_{01} = \sqrt{2^2 + 1^2}$ m and $L_{02} = \sqrt{2^2 + 0.5^2}$ m. The sensitivities of this system are well known because they were evaluated in previous research using different formulations and approaches [20, 19].

The ALI3-P formulation was used to conduct the sensitivity analysis of this mechanism with the following objective function, dependent on the solution of the dynamics equations

$$\psi = \int_{t_0}^{t_F} (\mathbf{r}_2 - \mathbf{r}_{20})^{\mathrm{T}} (\mathbf{r}_2 - \mathbf{r}_{20}) \, \mathrm{d}t \tag{36}$$

where $\mathbf{r}_2$ stands for the global position of point 2, $\mathbf{r}_{20}$ is the position of point 2 at time t_0, and t_F is set to 5 s. This objective function has an interesting physical interpretation: minimizing the objective function in Eq. (36) is equivalent to finding the natural lengths of the springs for

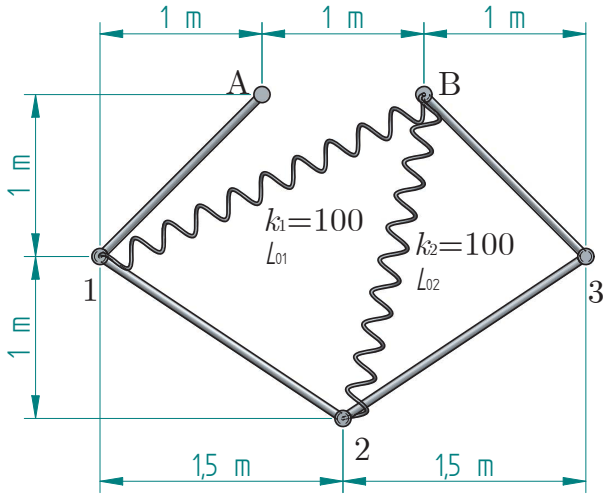

Figure 1: The five-bar mechanism used as test problem

which the initial position given in Fig. 1 is a static equilibrium configuration.

4.2 Nonholonomic two point-mass system

The second test example is a double point-mass system, shown in Fig. 2, and used in [16] to validate the ALI3-P formulation for systems with nonholonomic constraints. The two point masses move on the xy plane; the only external action on the system is the force f_B acting along the y direction on mass B, whose magnitude is chosen as parameter in this example.

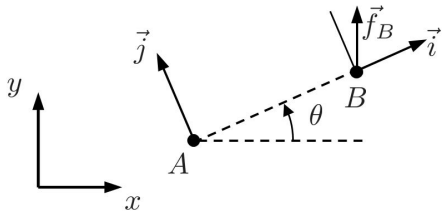

Figure 2: A double point-mass system featuring a nonholonomic constraint

The values of the point masses are $m_A = 5$ kg and $m_B = 7$ kg. The system motion can be described using five generalized coordinates, namely the x and y coordinates of points A and B and the angle θ between the global x-axis and the segment defined by points A and B, together with the holonomic constraint

$$\Phi = y_B - y_A - (x_B - x_A)\tan\theta = 0 \tag{37}$$

A nonholonomic constraint is added to enforce that the velocity of point A is always aligned with segment A-B

$$\check{\Phi} = (y_B - y_A)\,\dot{x}_A - (x_B - x_A)\,\dot{y}_A = 0 \tag{38}$$

Initially, $x_A = 1$ m, $x_B = 3$ m, $y_A = y_B = 1$ m, and both masses are moving with $\dot{x}_A = \dot{x}_B = 1$ m/s, while $\dot{y}_A = \dot{y}_B = 0$. The required output of this problem is the evaluation of the system sensitivities with respect to parameter $\rho = f_B$ during a 5 s forward-dynamics simulation.

4.3 Buggy vehicle

As a third test example, a full-scale three-dimensional vehicle model was developed, representing a four-wheeled buggy vehicle that features an articulated suspension system. This model consists of 18 rigid bodies, including the tubular framework, the wheels and the suspension parts. The multibody model is defined by means of natural, or fully Cartesian, coordinates plus some additional distance and angle coordinates (mixed coordinates). In total, 168 dependent coordinates are used, along with 154 constraints in order to enforce the rigid-body nature of each element and each kind of joint between each pair of bodies. This system features 14 degrees of freedom, namely six for the chassis, four for the suspension, and four more for each wheel. The steering mechanism does not introduce any additional degree of freedom since it is kinematically guided.

External forces acting on the vehicle, such as gravity, wheel-ground interactions, and braking and throttling actions on the wheels are considered. The vehicle follows a straight path at a constant speed over a flat terrain, until a transverse step is found at a certain distance from the starting point, and the wheels have to abruptly descend a step of 0.01 m. The purpose of the simulation is to compute the sensitivity of the system with respect to the natural length, the stiffness and the damping parameters

$$\boldsymbol{\rho}^{\mathrm{T}} = \left[k^{front}, k^{rear}, c^{front}, c^{rear}\right] \tag{39}$$

of the suspension of the front and rear wheels in order to minimize the fourth power vibration

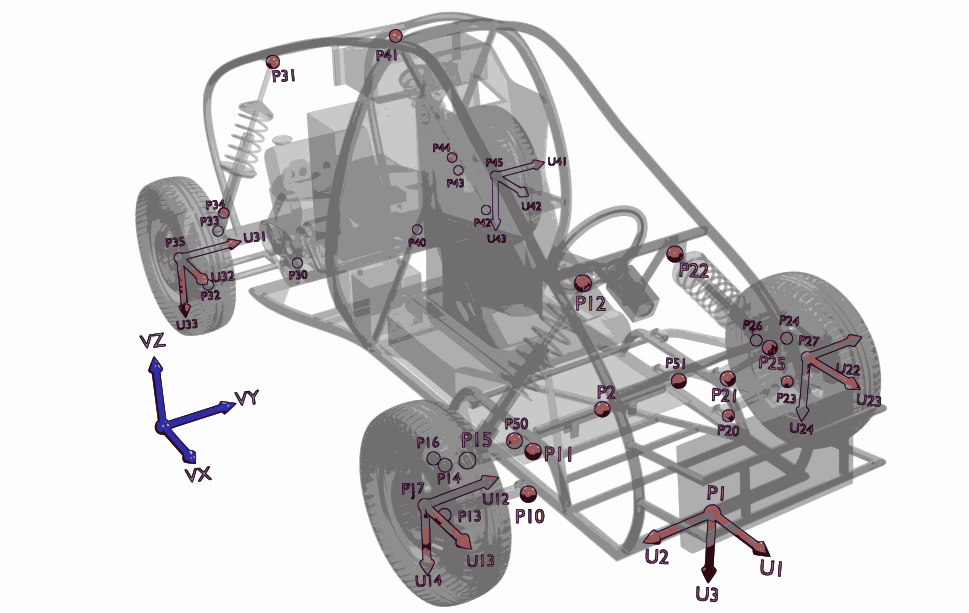

Figure 3: A view of the buggy vehicle, depicting the point and vector coordinates used in the numerical model

dose value of the chassis ψ, which is a measure of the riding comfort according to ISO 2631-1:

$$\psi = \int_{t_0}^{t_F} \ddot{z}^4 \, \mathrm{d}t \tag{40}$$

4.4 Reference formulations

The numerical results obtained with the ALI3-P formulation reported in Section 5 were validated against the solutions provided by sensitivity analysis formulations previously published in the literature. In particular, the index-1 DAE and penalty formulations with their corresponding sensitivity analysis equations described in [19] were used to provide reference results. The Matrix R formulation [20], was used as well to evaluate the correctness of the results for the vehicle in Section 4.3.

The index-1 DAE formulation obtains the system accelerations and Lagrange multipliers from the direct solution of the equations of motion

$$\begin{bmatrix} \mathbf{M} & \bar{\mathbf{A}}^{\mathrm{T}} \\ \bar{\mathbf{A}} & \mathbf{0} \end{bmatrix} \begin{bmatrix} \ddot{\mathbf{q}} \\ \boldsymbol{\lambda} \end{bmatrix} = \begin{bmatrix} \mathbf{Q} \\ -\dot{\bar{\mathbf{A}}}\dot{\mathbf{q}} - \dot{\bar{\mathbf{b}}} \end{bmatrix} \tag{41}$$

The numerical integration of Eq. (41) will lead to drift-off errors because the kinematic constraints are not stabilized. The penalty formulation solves this problem by making the Lagrange multipliers proportional to the violation of constraints at the configuration, velocity, and acceleration levels, which reduces the system of DAEs in Eq. (41) to a system of ODEs

$$\bar{\mathbf{M}}\ddot{\mathbf{q}} = \bar{\mathbf{Q}} \tag{42}$$

where

$$\bar{\mathbf{M}} = \mathbf{M} + \bar{\mathbf{A}}^{\mathrm{T}}\boldsymbol{\alpha}\bar{\mathbf{A}} \tag{43a}$$

$$\bar{\mathbf{Q}} = \mathbf{Q} - \bar{\mathbf{A}}^{\mathrm{T}}\boldsymbol{\alpha}\left(\dot{\bar{\mathbf{A}}}\dot{\mathbf{q}} + \dot{\bar{\mathbf{b}}} + 2\omega\xi\left(\bar{\mathbf{A}}\dot{\mathbf{q}} + \bar{\mathbf{b}}\right)\right) + \omega^2\boldsymbol{\Phi}_{\mathbf{q}}^{\mathrm{T}}\boldsymbol{\alpha}\boldsymbol{\Phi} \tag{43b}$$

Terms ξ and ω are stabilization parameters that play a role similar to those in Baumgarte's method [4].

The direct sensitivity analysis equations for the index-1 DAE formulation are

$$\begin{bmatrix} \mathbf{M} & \bar{\mathbf{A}}^{\mathrm{T}} \\ \bar{\mathbf{A}} & \mathbf{0} \end{bmatrix} \begin{bmatrix} \ddot{\mathbf{q}}_{\rho} \\ \boldsymbol{\lambda}_{\rho} \end{bmatrix} = \begin{bmatrix} \mathbf{Q}_{\rho} - \mathbf{M}_{\rho}\ddot{\mathbf{q}} - \bar{\mathbf{A}}_{\rho}^{\mathrm{T}}\boldsymbol{\lambda} - \mathbf{C}\dot{\mathbf{q}}_{\rho} - \left(\mathbf{M}_{\mathbf{q}}\ddot{\mathbf{q}} + \bar{\mathbf{A}}_{\mathbf{q}}^{\mathrm{T}}\boldsymbol{\lambda} + \mathbf{K}\right)\mathbf{q}_{\rho} \\ \mathbf{c}_{\rho} - \bar{\mathbf{A}}_{\rho}\ddot{\mathbf{q}} + \mathbf{c}_{\dot{\mathbf{q}}}\dot{\mathbf{q}}_{\rho} - \left(\bar{\mathbf{A}}_{\mathbf{q}}\ddot{\mathbf{q}} - \mathbf{c}_{\mathbf{q}}\right)\mathbf{q}_{\rho} \end{bmatrix} \tag{44}$$

where

$$\mathbf{c}_{\mathbf{q}} = -\dot{\bar{\mathbf{A}}}_{\mathbf{q}}\dot{\mathbf{q}} - \dot{\bar{\mathbf{b}}}_{\mathbf{q}} \tag{45a}$$

$$\mathbf{c}_{\dot{\mathbf{q}}} = -\bar{\mathbf{A}}_{\mathbf{q}}\dot{\mathbf{q}} - \dot{\bar{\mathbf{A}}} - \bar{\mathbf{b}}_{\mathbf{q}} \tag{45b}$$

$$\mathbf{c}_{\rho} = -\dot{\bar{\mathbf{A}}}_{\rho}\dot{\mathbf{q}} - \dot{\bar{\mathbf{b}}}_{\rho} \tag{45c}$$

The expression of the gradient $\nabla_{\rho}\psi$ for the index-1 DAE formulation is

$$\begin{aligned} \nabla_{\rho}\psi^{\mathrm{T}} = {} & \left(w_{\mathbf{q}}\mathbf{q}_{\rho} + w_{\dot{\mathbf{q}}}\dot{\mathbf{q}}_{\rho} + w_{\ddot{\mathbf{q}}}\ddot{\mathbf{q}}_{\rho} + w_{\boldsymbol{\lambda}}\boldsymbol{\lambda}_{\rho} + w_{\rho}\right)_F + \\ & \int_{t_0}^{t_F}\left(g_{\mathbf{q}}\mathbf{q}_{\rho} + g_{\dot{\mathbf{q}}}\dot{\mathbf{q}}_{\rho} + g_{\ddot{\mathbf{q}}}\ddot{\mathbf{q}}_{\rho} + g_{\boldsymbol{\lambda}}\boldsymbol{\lambda}_{\rho} + g_{\rho}\right)\mathrm{d}t \end{aligned} \tag{46}$$

The direct sensitivity analysis equations for the penalty method read

$$\bar{\mathbf{M}}\ddot{\mathbf{q}}_{\rho} + \bar{\mathbf{C}}\dot{\mathbf{q}}_{\rho} + \left(\bar{\mathbf{K}} + \bar{\mathbf{M}}_{\mathbf{q}}\ddot{\mathbf{q}}\right)\mathbf{q}_{\rho} = \bar{\mathbf{Q}}_{\rho} - \bar{\mathbf{M}}_{\rho}\ddot{\mathbf{q}} \tag{47}$$

where

$$\bar{\mathbf{K}} = -\frac{\partial \bar{\mathbf{Q}}}{\partial \mathbf{q}}, \qquad \bar{\mathbf{C}} = -\frac{\partial \bar{\mathbf{Q}}}{\partial \dot{\mathbf{q}}} \tag{48}$$

The objective function for the penalty formulation may include terms that depend on its approximate Lagrange multipliers $\boldsymbol{\lambda}^*$ [38]

$$\psi = w\left(\mathbf{q}_F, \dot{\mathbf{q}}_F, \ddot{\mathbf{q}}_F, \boldsymbol{\rho}_F, \boldsymbol{\lambda}_F^*\right) + \int_{t_0}^{t_F} g\left(\mathbf{q}, \dot{\mathbf{q}}, \ddot{\mathbf{q}}, \boldsymbol{\rho}, \boldsymbol{\lambda}^*\right) \mathrm{dt} \tag{49}$$

Accordingly, the expression of gradient $\nabla_{\boldsymbol{\rho}}\psi$ in this case is

$$\begin{aligned} \nabla_{\boldsymbol{\rho}}\psi^{\mathrm{T}} = \frac{\mathrm{d}\psi}{\mathrm{d}\boldsymbol{\rho}} = &\left[w_{\mathbf{q}}\mathbf{q}_{\boldsymbol{\rho}} + w_{\dot{\mathbf{q}}}\dot{\mathbf{q}}_{\boldsymbol{\rho}} + w_{\ddot{\mathbf{q}}}\ddot{\mathbf{q}}_{\boldsymbol{\rho}} + w_{\boldsymbol{\rho}} + w_{\boldsymbol{\lambda}^*}\boldsymbol{\lambda}_{\boldsymbol{\rho}}^*\right]_F + \\ &\int_{t_0}^{t_F} \left[g_{\mathbf{q}}\mathbf{q}_{\boldsymbol{\rho}} + g_{\dot{\mathbf{q}}}\dot{\mathbf{q}}_{\boldsymbol{\rho}} + g_{\ddot{\mathbf{q}}}\ddot{\mathbf{q}}_{\boldsymbol{\rho}} + g_{\boldsymbol{\rho}} + g_{\boldsymbol{\lambda}^*}\boldsymbol{\lambda}_{\boldsymbol{\rho}}^*\right] \mathrm{dt} \end{aligned} \tag{50}$$

where

$$\boldsymbol{\lambda}_{\boldsymbol{\rho}}^* = \boldsymbol{\alpha}\left(\frac{\mathrm{d}\dot{\tilde{\boldsymbol{\Phi}}}}{\mathrm{d}\boldsymbol{\rho}} + 2\xi\omega\frac{\mathrm{d}\bar{\boldsymbol{\Phi}}}{\mathrm{d}\boldsymbol{\rho}} + \omega^2\frac{\mathrm{d}\tilde{\boldsymbol{\Phi}}}{\mathrm{d}\boldsymbol{\rho}}\right), \tag{51a}$$

$$\begin{aligned} \frac{\mathrm{d}\dot{\bar{\boldsymbol{\Phi}}}}{\mathrm{d}\boldsymbol{\rho}} =& \bar{\mathbf{A}}\ddot{\mathbf{q}}_{\boldsymbol{\rho}} + \left(\bar{\mathbf{A}}_{\mathbf{q}}\dot{\mathbf{q}} + \dot{\bar{\mathbf{A}}} + \bar{\mathbf{b}}_{\mathbf{q}}\right)\dot{\mathbf{q}}_{\boldsymbol{\rho}} \\ &+ \left(\bar{\mathbf{A}}_{\mathbf{q}}\ddot{\mathbf{q}} + \left(\dot{\bar{\mathbf{A}}}\right)_{\mathbf{q}}\dot{\mathbf{q}} + \left(\dot{\bar{\mathbf{b}}}\right)_{\mathbf{q}}\right)\mathbf{q}_{\boldsymbol{\rho}} + \bar{\mathbf{A}}_{\boldsymbol{\rho}}\ddot{\mathbf{q}} + \left(\dot{\bar{\mathbf{A}}}\right)_{\boldsymbol{\rho}}\dot{\mathbf{q}} + \left(\dot{\bar{\mathbf{b}}}\right)_{\boldsymbol{\rho}}, \end{aligned} \tag{51b}$$

$$\frac{\mathrm{d}\bar{\boldsymbol{\Phi}}}{\mathrm{d}\boldsymbol{\rho}} = \bar{\mathbf{A}}\dot{\mathbf{q}}_{\boldsymbol{\rho}} + \left(\bar{\mathbf{A}}_{\mathbf{q}}\dot{\mathbf{q}} + \bar{\mathbf{b}}_{\mathbf{q}}\right)\mathbf{q}_{\boldsymbol{\rho}} + \bar{\mathbf{A}}_{\boldsymbol{\rho}}\dot{\mathbf{q}} + \bar{\mathbf{b}}_{\boldsymbol{\rho}}, \tag{51c}$$

$$\frac{\mathrm{d}\tilde{\boldsymbol{\Phi}}}{\mathrm{d}\boldsymbol{\rho}} = \bar{\mathbf{A}}\mathbf{q}_{\boldsymbol{\rho}} + \tilde{\boldsymbol{\Phi}}_{\boldsymbol{\rho}}, \tag{51d}$$

$$\tilde{\boldsymbol{\Phi}} = \begin{bmatrix} \boldsymbol{\Phi} \\ \\ \mathbf{0}_{\check{m}\times 1} \end{bmatrix} \tag{51e}$$

The Matrix R formulation for holonomic systems transforms the original DAE into a set of ODEs by means of the following transformations of velocities and accelerations,

$$\dot{\mathbf{q}} = \mathbf{R}\dot{\mathbf{z}} - \mathbf{S}\boldsymbol{\Phi}_t \tag{52a}$$

$$\ddot{\mathbf{q}} = \mathbf{R}\ddot{\mathbf{z}} - \mathbf{S}\left(\dot{\boldsymbol{\Phi}}_{\mathbf{q}}\dot{\mathbf{q}} - \dot{\boldsymbol{\Phi}}_t\right) = \mathbf{R}\ddot{\mathbf{z}} + \mathbf{S}\mathbf{c} \tag{52b}$$

where $\dot{\mathbf{z}}$ is a set of independent generalized velocities and matrices $\mathbf{S}$ and $\mathbf{R}$ are, respectively,

a right inverse of the constraints Jacobian matrix, $\mathbf{\Phi_q}$, and a basis of its nullspace, if no redundant constraints are present. Only holonomic constraints were considered in Eqs. (52) for the sake of simplicity, because the extension of this formulation to nonholonomic systems is not straightforward.

The dependent velocities, accelerations and virtual displacements can be expressed in terms of the independent degrees of freedom by means of these matrices to write the system dynamics equations as:

$$\left(\mathbf{R}^{\mathrm{T}}\mathbf{M}\mathbf{R}\right)\ddot{\mathbf{z}} = \mathbf{R}^{\mathrm{T}}\left(\mathbf{Q} - \mathbf{M}\mathbf{S}\mathbf{c}\right) \tag{53}$$

which is a system of ODEs whose size equals the number of degrees of freedom of the system. The detailed expression of the sensitivity analysis terms for the Matrix R formulation is provided in [20].

5 Results

The methods described in Sections 2–3 were implemented as MATLAB code and applied to the simulation of the first two numerical experiments in Sections 4.1 and 4.2 using MATLAB R2016a 64-bit. The method described in Section 3 was also implemented as a general sensitivity formulation in the framework of MBSLIM [18] in Fortran 2008 and applied to the simulation of the buggy vehicle in Section 4.3. The ALI3-P formulation for the dynamics, described in Section 2, was already available in MBSLIM. The numerical experiments were performed running the code in an Intel Core i7-6700K CPU at 4.00 GHz running Windows 10 Pro built with Fortran Intel Parallel Studio XE 2018.

5.1 Five-bar mechanism

The 5 s forward-dynamics simulation of the motion of the five-bar linkage was carried out with the ALI3-P formulation with an integration step-size $h = 10^{-2}$ s. A single penalty factor $\alpha = 10^{7}$ was applied to all the kinematic constraints. The values of the integration constants were adjusted to $\beta = 0.25$ and $\gamma = 0.5$ so that Eqs. (7) and (34) matched the trapezoidal

rule scheme. The integrator tolerance was set to 10^{-12}, limiting with this value the maximum admissible difference in the norm of the integration variables between two consecutive solver iterations. The number of velocity and acceleration projections per time-step was set to five. The sensitivity analysis was conducted immediately after each integration time-step was completed.

The simulation was repeated using the penalty formulation in Eq. (42) and the trapezoidal rule in a Newton-Raphson iteration scheme to integrate the motion and the corresponding sensitivity equations (47). The same penalty factor and tolerances as in the ALI3-P case were used. The stabilization parameters were set to $\xi = 1$ and $\omega = 10$.

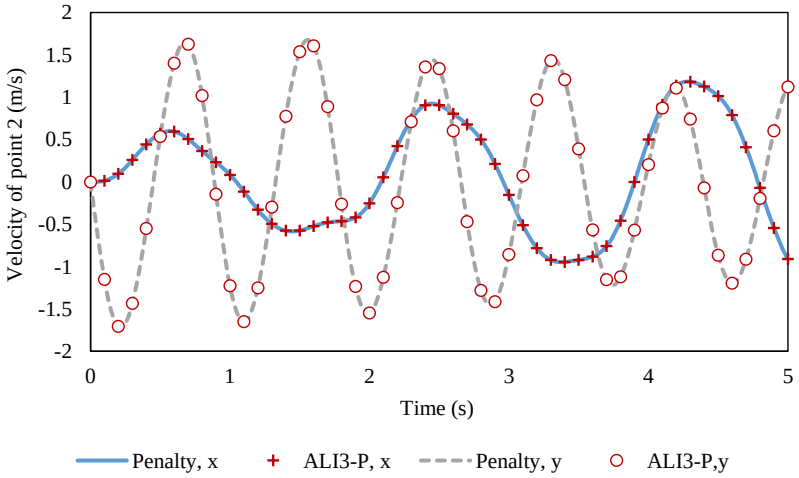

Figure 4: Time-history of the x- and y-velocity components of point 2 of the five-bar linkage

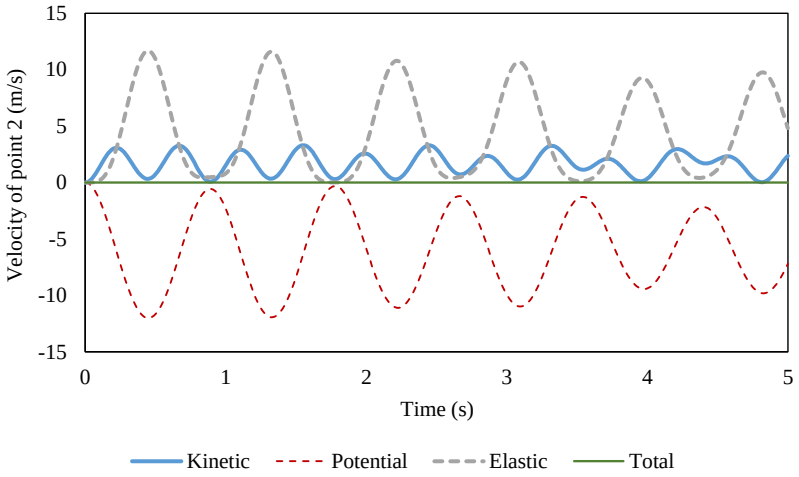

Figure 5: Components of the mechanical energy of the five-bar linkage

Both methods delivered very similar results in the integration of the dynamics. Fig. 4 shows the x- and y- components of the velocity of point 2 obtained with each formulation. Fig. 5

contains the time-history of the kinetic, potential gravitatory and potential elastic energies of the mechanism. All the forces that act on the system are conservative; accordingly, the mechanical energy remained constant during motion. The obtained results matched those obtained with other formulations, such as velocity projection methods, reported in [20].

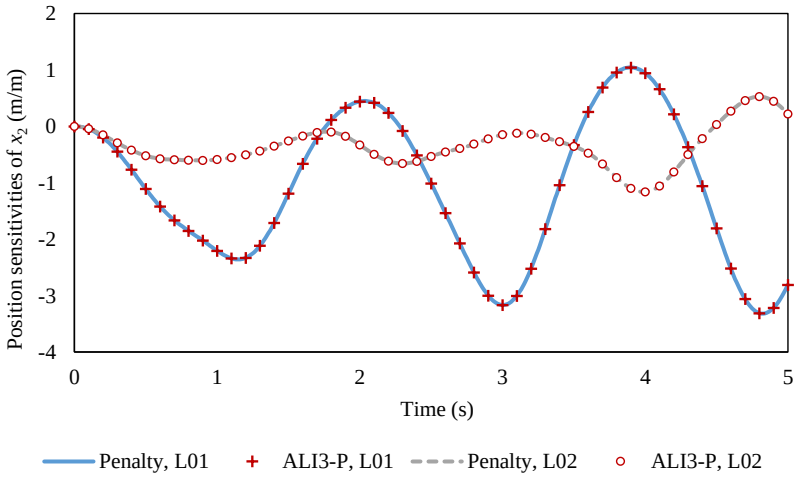

Figure 6: Sensitivities $x_{2,L_{01}}$ and $x_{2,L_{02}}$ of the x coordinate of point 2 in the five-bar linkage with respect to the system parameters

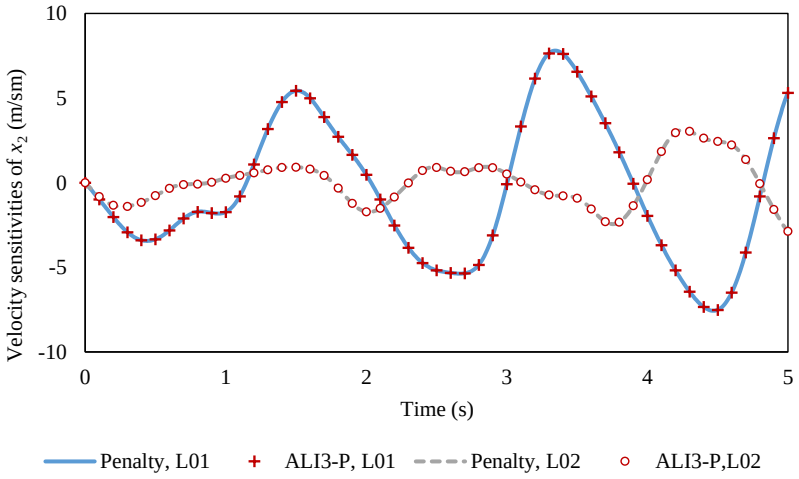

Figure 7: Sensitivities $\dot{x}_{2,L_{01}}$ and $\dot{x}_{2,L_{02}}$ of the x component of the velocity of point 2 in the five-bar linkage with respect to the system parameters

Figures 6–8 show the time-history of the sensitivities of the x-coordinate of point 2 at the configuration, velocity, and acceleration levels, with respect to the system parameters L_{01} and L_{02}. The gradient $\nabla_{\boldsymbol{\rho}}\psi = [\ \mathrm{d}\psi/\mathrm{d}L_{01},\quad \mathrm{d}\psi/\mathrm{d}L_{02}\ ]$ obtained upon completion of the integration of the sensitivities at time $t_F = 5$ s with the ALI3-P formulation was $\nabla_{\boldsymbol{\rho}}\psi = [\ -4.2294,\quad 3.2112\ ]$. The penalty formulation yielded $\nabla_{\boldsymbol{\rho}}\psi = [\ -4.2294,\quad 3.2111\ ]$. These results fall within the range

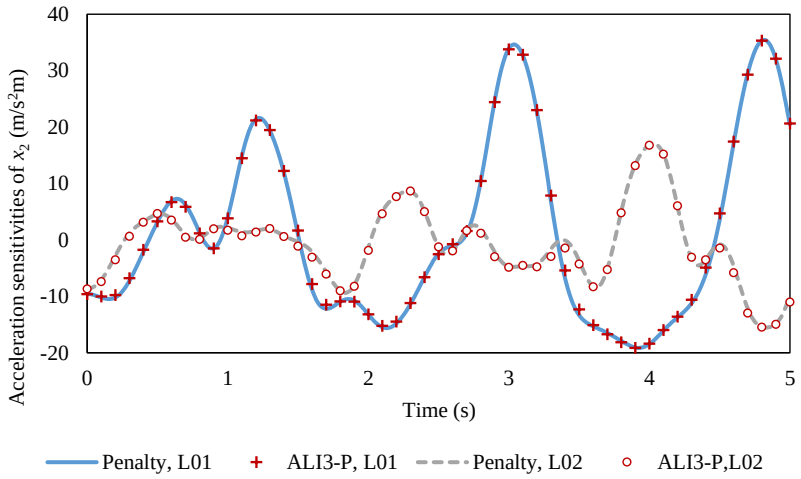

Figure 8: Sensitivities $\ddot{x}_{2,L_{01}}$ and $\ddot{x}_{2,L_{02}}$ of the x component of the acceleration of point 2 in the five-bar linkage with respect to the system parameters

reported in [19].

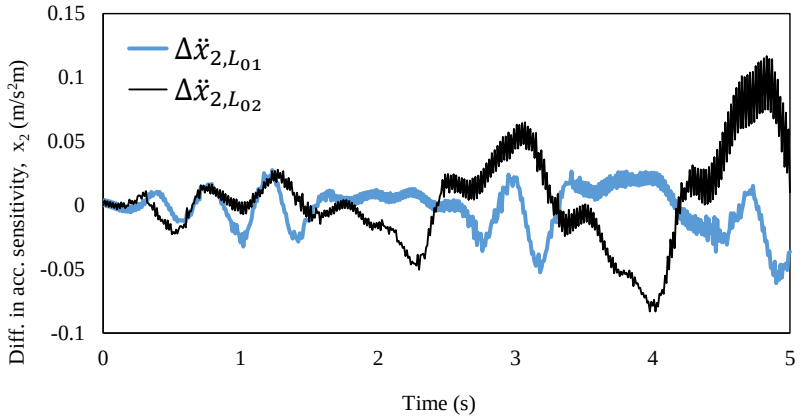

Figure 9: Differences introduced in the sensitivities of acceleration $\ddot{x}_2$ of the five-bar linkage when the sensitivity analysis is carried out without velocity and acceleration projections

It must be mentioned that the five-bar linkage is subjected only to holonomic constraints and, accordingly, the contribution of the velocity and acceleration projections in Eqs. (26) and (27) to the sensitivity analysis is relatively small. The corrections introduced in $\dot{\mathbf{q}}_{\boldsymbol{\rho}}$ and $\ddot{\mathbf{q}}_{\boldsymbol{\rho}}$ by the projections do not modify significantly the values $\dot{\mathbf{q}}^*_{\boldsymbol{\rho}}$ and $\ddot{\mathbf{q}}^*_{\boldsymbol{\rho}}$ obtained after the solution of the TLM in Eq. (35). Fig. 9 shows the differences in the sensitivities of the x-component of the acceleration of point 2 when the velocity and acceleration projections are omitted altogether during the analysis. The gradient of the objective function obtained at the end of the integration process was also modified slightly, its new value being $\nabla_{\boldsymbol{\rho}}\psi = [\ -4.2276,\ \ 3.2062\ ]$. In systems with nonholonomic constraints, however, the sensitivity of the projections could not

be neglected, because these constraints are not enforced by the Newton-Raphson iteration in Eq. (9), as discussed in Section 5.2. This would also be the case in systems with rheonomic constraints.

5.2 Nonholonomic two point-mass system

The forward-dynamics simulation of the 5 s motion of the double point-mass system was carried out with the ALI3-P formulation using an integration step-size $h = 10^{-3}$ s. Every other parameter in the method was assigned the same value as in Section 5.1. The dynamics was also simulated with the penalty formulation, with $h = 10^{-3}$ s, $\alpha = 10^5$, $\xi = 1$, and $\omega = 10$, using the trapezoidal rule as integrator with a tolerance of 10^{-12}.

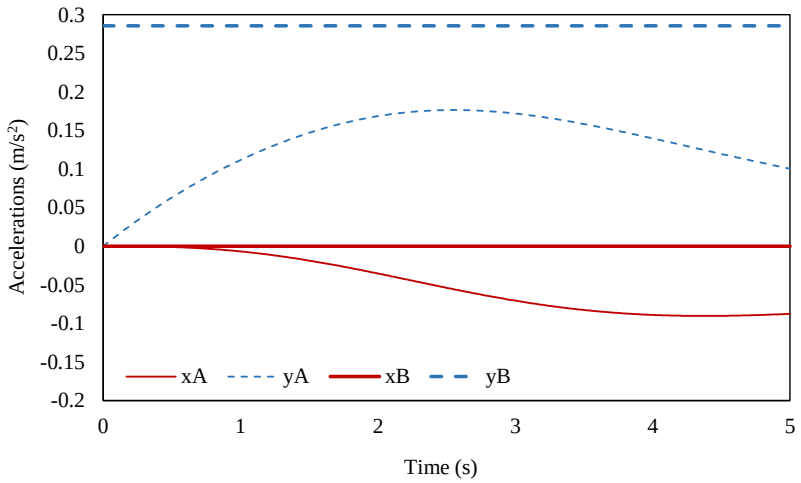

Figure 10: Accelerations of points A and B during motion of the double point-mass system

Figure 10 shows the accelerations of points A and B in the double point-mass system; both methods delivered almost identical results. As expected, the acceleration of point B does not change with time.

After completing the integration of the dynamics, the sensitivity analysis of this problem was carried out with the ALI3-P algorithm in Section 3.1 and compared to the results delivered by the index-1 DAE method in Eq. (44). The results are summarized in Fig. 11. Both formulations resulted in identical sensitivities in practice. It must be noted that the projection steps in Eqs. (26) and (27) are now absolutely necessary to correctly evaluate the sensitivities of the velocities and the accelerations, $\dot{\mathbf{q}}_\rho$ and $\ddot{\mathbf{q}}_\rho$, if the ALI3-P method is used. The nonholonomic

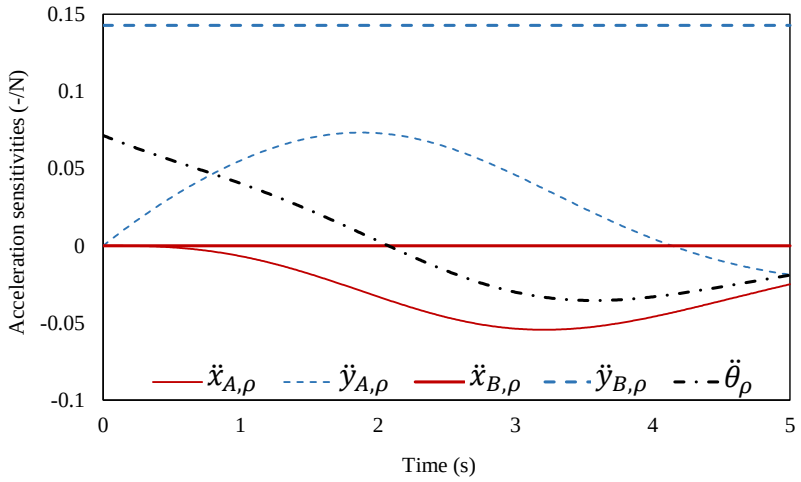

Figure 11: Acceleration-level sensitivities of the double point-mass system

kinematic constraint (38) does not enter in the TLM in Eq. (35) and the integration scheme in Eqs. (34) consistently returns $\ddot{x}_A^* = 0$ and $\ddot{y}_A^* = 0$ during the whole motion. The correct values of $\ddot{x}_A$ and $\ddot{y}_A$, shown in Fig. 11, were imposed entirely during the projection step in Eqs. (27). The corrections introduced by the projections were also necessary to properly evaluate the acceleration-level sensitivity of angle θ, $\ddot{\theta}_\rho$, and the velocity-level sensitivities $\dot{x}_{A,\rho}$, $\dot{y}_{A,\rho}$, and $\dot{\theta}_\rho$.

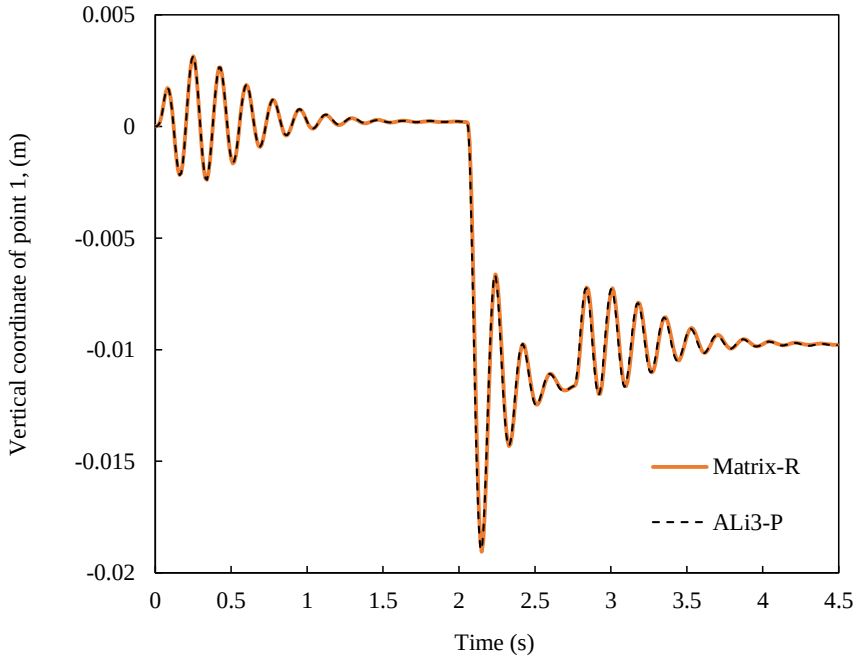

Figure 12: Vertical coordinate of point 1 during the buggy vehicle maneuver

5.3 Buggy vehicle

The first 4.5 s of the maneuver described in Section 4.3 were simulated using the ALI3-P and the Matrix R methods, both implemented in Fortran in the MBSLIM library. The sensitivity terms and the objective function in Eq. (40) were obtained as well. The integration step-size was set to $h = 10^{-3}\,\mathrm{s}$, and the penalty factor of the ALI3-P formulation, to $\alpha = 10^{10}$. The rest of the parameters of the method matched the values of the Section 5.1.

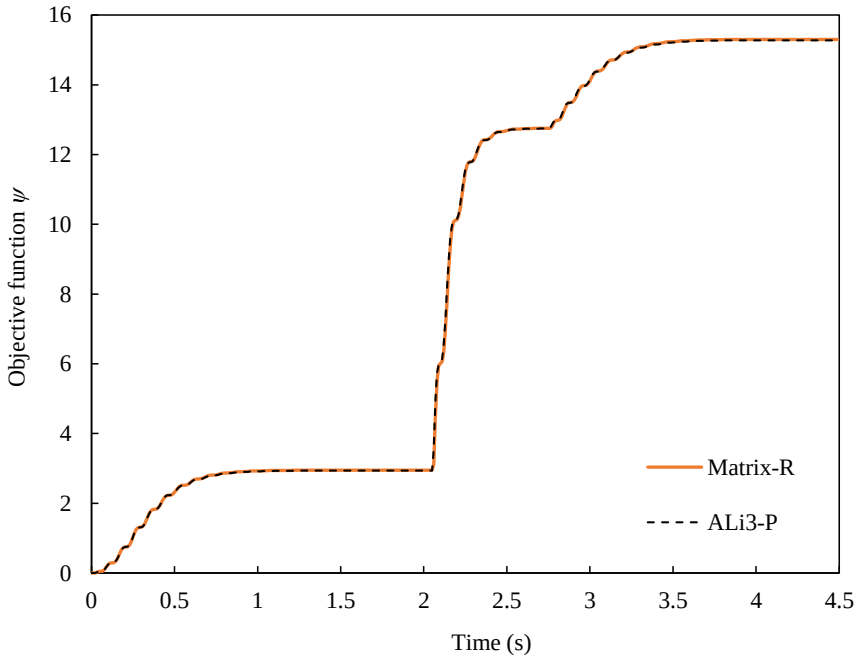

Figure 13: Value of the objective function ψ during the buggy vehicle maneuver

Figure 12 shows the vertical coordinate of point 1 of the vehicle, evaluated using both methods. The value of the objective function ψ is depicted in Fig. 13. Figure 14 details the evolution of the sensitivities $\partial\psi/\partial\boldsymbol{\rho}$ during the simulation.

In both cases, the ALI3-P and Matrix R methods delivered practically the same results, which confirms the correctness of the ALI3-P sensitivity equations. The small differences observed between both formulations come from the slightly higher numerical damping introduced in the dynamics of the vehicle by the ALI3-P formulation, compared to Matrix R.

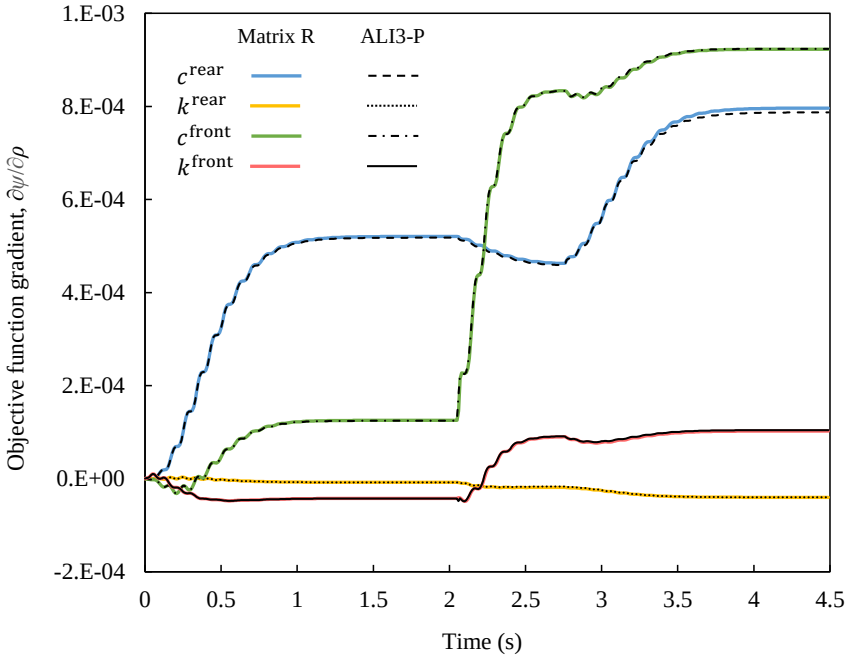

Figure 14: Sensitivities of the objective function ψ with respect to the system parameters $\boldsymbol{\rho}$ during the buggy vehicle maneuver

6 Discussion

The correctness of the direct sensitivity analysis described in Section 3 relies on the accurate solution of the forward-dynamics problem. The ALI3-P algorithm presented in Section 2 has been proven to be more robust to parameter changes than its penalty and index-1 DAE counterparts in the forward-dynamics simulation of mechanical systems [29]. It can also deal, without special adjustments, with systems that undergo singular configurations, which is not the case of conventional velocity-transformation based methods. On the other hand, the tangent matrix used by the ALI3-P algorithm has been shown to become ill-conditioned when the integration step-size of the method, h, is reduced [13].

In this section, the effect of the most relevant integration and formulation parameters on the accuracy of the sensitivity analysis of the ALI3-P method is discussed. The obtained results were compared to those yielded by the sensitivity analysis of the reference methods in Section 4.4.

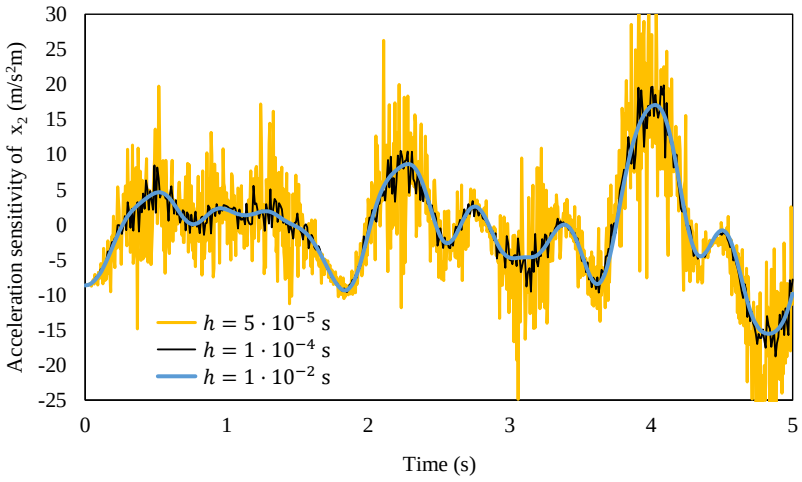

Figure 15: Sensitivity $\ddot{x}_{2,L_{02}}$ of acceleration $\ddot{x}_2$ of the five-bar linkage with respect to parameter L_{02}, evaluated with the penalty formulation and different values of the integration step-size h

6.1 Integration parameters

The integration step-size h usually has an important effect on the accuracy of the results obtained in forward-dynamics simulations. The configuration-level Newton-Raphson iteration of the ALI3-P method enables it to obtain accurate results for relative large integration step-sizes. Conversely, when the step-size decreases, its tangent matrix may become ill-conditioned, and the accuracy of the integration, compromised.

Table 1: Effect of integration step-size h on the gradient of the objective function of the five-bar example

h (s)	ALI3-P	Penalty
10^{-1}	$[-4.1458, 3.0476]$	$[\mathrm{NaN}, \mathrm{NaN}]$
$5 \cdot 10^{-2}$	$[-4.2340, 3.1865]$	$[-4.3059, 4.1385]$
10^{-2}	$[-4.2294, 3.2112]$	$[-4.2294, 3.2111]$
$5 \cdot 10^{-3}$	$[-4.2290, 3.2116]$	$[-4.2290, 3.2115]$
10^{-3}	$[-4.2291, 3.2115]$	$[-4.2293, 3.2112]$
$5 \cdot 10^{-4}$	$[-4.2296, 3.2108]$	$[-4.2305, 3.2196]$
10^{-4}	$[-4.2313, 3.2063]$	$[-4.2278, 3.2435]$
$5 \cdot 10^{-5}$	$[-4.2334, 3.2002]$	$[-4.2658, 3.3159]$
10^{-5}	$[-4.2271, 3.2063]$	$[-3.5680, 2.3032]$

Table 1 shows the values of the gradient $\nabla_{\boldsymbol{\rho}}\psi$ for the five-bar linkage obtained with the ALI3-P method for different values of the integration step-size h. All the other method parameters retained the values assigned to them in Section 5. The method remained stable and accurate for step-sizes as low as 10^{-5} s, although at the cost of increasing the number of iterations required

during the Newton-Raphson procedure. The results obtained with the penalty formulation are shown as well. It must be noted that, regardless of the integration step-size, both methods were able to correctly carry out the forward-dynamics simulation of the mechanism motion; however, the penalty method only delivered correct sensitivities when 10^{-4} s $\leq h \leq 10^{-2}$ s. Fig. 15 illustrates the degradation of the acceleration-level sensitivity $\ddot{x}_{2,L_{02}}$ evaluated with the penalty formulation for small step-sizes h. The ALI3-P method did not suffer from this problem in the studied range of h.

The integration step-size was also varied between $h = 10^{-1}$ s and $h = 10^{-5}$ s in the evaluation of the sensitivities of the double mass example. The methods and parameters were kept the same as in Section 5.2; in all cases the results of the forward-dynamics simulation were practically the same. The ALI3-P method delivered correct sensitivities for the whole range of h, while its index-1 DAE counterpart yielded wrong acceleration-level sensitivities for $h \leq 10^{-4}$ s.

Table 2: Effect of integrator tolerance on the gradient of the objective function of the five-bar example

Tolerance (m)	ALI3-P	Penalty
10^{-12}	$[-4.2294, 3.2112]$	$[-4.2294, 3.2111]$
10^{-11}	$[-4.2297, 3.2117]$	$[-4.2287, 3.2110]$
10^{-10}	$[-4.2297, 3.2115]$	$[-4.2298, 3.2157]$
10^{-9}	$[-4.2400, 3.2113]$	$[-4.1707, 3.2049]$
10^{-8}	$[-4.3320, 3.2303]$	$[-4.3133, 3.3029]$
10^{-7}	$[-4.3320, 3.2304]$	Did not converge

Regarding robustness with respect to changes in integration tolerances, the ALI3-P method also showed a superior behaviour when compared to the reference formulations. The gradients obtained for different maximum admissible errors in the iteration process of the five-bar linkage are compared in Table 2.

6.2 Formulation parameters

The penalty factor α is the only formulation parameter present in the ALI3-P, the index-1 DAE, and the penalty methods. Using large penalty factors usually improves the convergence rate of the algorithms, leading to faster computations. However, the integration procedure may become unstable if α goes beyond a certain threshold. In the five-bar linkage, the ALI3-P method obtained correct sensitivities for $\alpha \leq 10^{10}$, while the penalty method required the use of $\alpha \leq 10^{8}$.

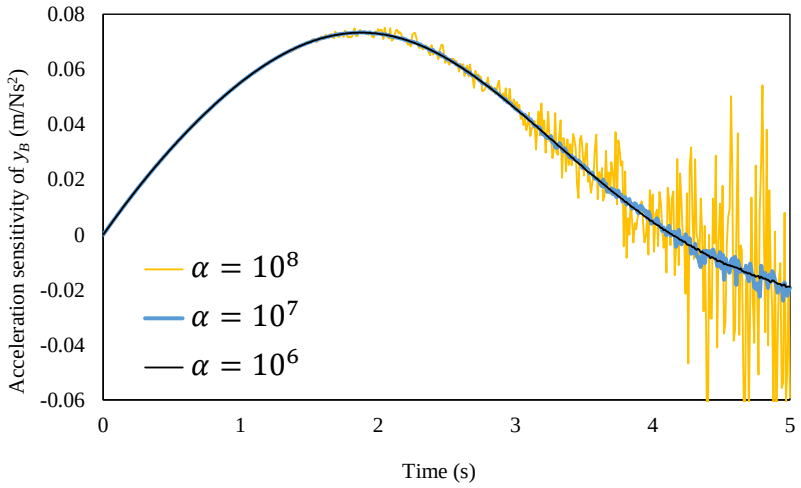

Figure 16: Sensitivity $\ddot{y}_{A,\rho}$ of acceleration $\ddot{y}_A$ in the double point-mass system, evaluated with the index-1 DAE formulation for different values of the penalty factor α

Regarding the double mass example with the nonholonomic constraint, the selection of factor α in the solution of the dynamics with Eqs. (42) and (43) was found to have a significant effect on the sensitivity analysis results delivered by the index-1 DAE formulation. Although the dynamics of the double point-mass assembly was correctly integrated, and no noticeable differences could be appreciated in the values of $\mathbf{q}$, $\dot{\mathbf{q}}$, and $\ddot{\mathbf{q}}$ during motion, instabilities were introduced in the evaluated sensitivities $\ddot{\mathbf{q}}_{\boldsymbol{\rho}}$ for penalty factors $\alpha \geq 10^6$, as illustrated in Fig. 16. Conversely, varying the penalty factor up to $\alpha = 10^{10}$ did not affect the sensitivities yielded by the ALI3-P formulation.

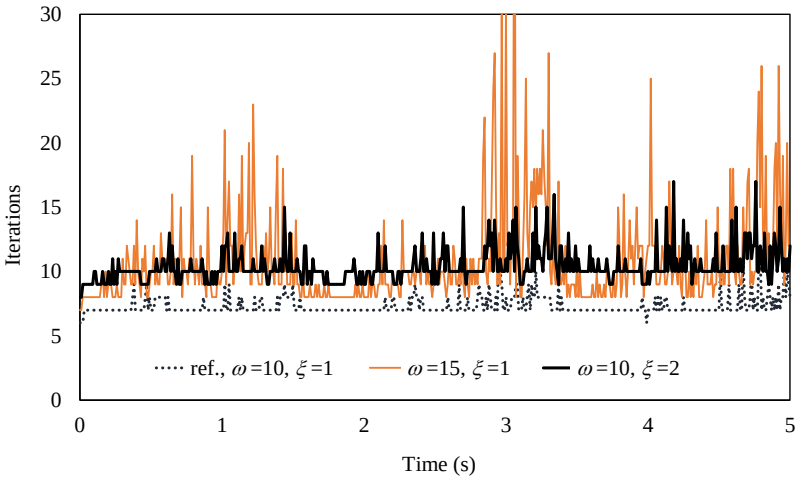

Figure 17: Number of iterations required by the trapezoidal rule to achieve convergence in the evaluation of the sensitivities of the five-bar linkage, with the penalty formulation and different values of the stabilization parameters ξ and ω

Another important difference between the ALI3-P method and the index-1 DAE and penalty algorithm used for comparison is the way in which kinematic constraints are enforced. The ALI3-P algorithm uses mass-orthogonal projections to obtain sets of generalized velocities and accelerations that comply with the constraints. The index-1 DAE and the penalty formulations resort to Baumgarte stabilization, instead, which requires the selection of appropriate values of parameters ξ and ω [22]. Simulation results confirmed that selecting low values for ξ and ω may lead to an inaccurate fulfillment of the kinematic constraints. Increasing their values, although not affecting noticeably the computed sensitivities, has a negative effect on the convergence rate of the algorithms, causing them to iterate longer to converge to similar results and significantly reducing computational efficiency. For instance, obtaining the sensitivities of the five-bar linkage with the parameters set in Section 5.1 needed an average of 7.3 iterations of the integrator per time-step. Raising ω from 10 to 25 delivered practically the same solution for the dynamics and the sensitivities, but an average of 74.3 iterations were required per time-step instead. The number of necessary convergence iterations to meet the same tolerances exceeded 500 several times. Less severe cases are illustrated in Fig. 17.

The optimum values for ξ and ω depend on the dynamic response of the mechanical system, and finding them often leads to a time consuming trial-and-error tuning procedure. This problem is avoided with the ALI3-P method, because the satisfaction of the kinematic constraints at velocity and acceleration levels is ensured by the projections in Eqs. (13) and (15). For the correction of velocity- and acceleration- level sensitivities, Eqs. (26) and (27) are used. In the examples discussed in this paper, two projection iterations were enough to arrive at correct sensitivities. Increasing the number of projection iterations beyond two did not result in the improvement of the results.

6.3 Performance comparison

The vehicle example in Section 4.3 was used to compare the performance of the ALI3-P and Matrix R methods. Integration step-sizes $h = 10^{-2}\,\mathrm{s}$ and $h = 10^{-3}\,\mathrm{s}$ were used for the comparison. The results obtained with $h = 10^{-2}\,\mathrm{s}$ matched closely those shown in Figs. 12–14. For the same integration step-size, the ALI3-P formulation exhibited noticeably shorter computation elapsed times. Table 3 shows that both formulations are above real-time performance when $h = 10^{-2}\,\mathrm{s}$, but even in that case the ALI3-P is about 2.5 times faster in this example.

	h = 10^{-2} s	h = 10^{-3} s
ALI3-P	1.672	10.500
Matrix R	4.141	34.781

Table 3: Elapsed times (s) in the simulation and sensitivity analysis of the buggy maneuver

Table 4 illustrates the fact that both formulations delivered very similar results regardless of the integration step-size used. Each of the columns displays the sensitivity of the objective function with respect to a system parameter p, where $\psi_p = \partial\psi/\partial p$.

	h(s)	$\psi_{k\,front}$	$\psi_{c\,front}$	$\psi_{k\,rear}$	$\psi_{c\,rear}$
ALI3-P	10^{-2}	$9.496 \cdot 10^{-5}$	$9.303 \cdot 10^{-4}$	$-3.553 \cdot 10^{-5}$	$7.927 \cdot 10^{-4}$
	10^{-3}	$1.090 \cdot 10^{-4}$	$9.401 \cdot 10^{-4}$	$-3.663 \cdot 10^{-5}$	$7.636 \cdot 10^{-4}$
Matrix R	10^{-2}	$9.580 \cdot 10^{-5}$	$9.293 \cdot 10^{-4}$	$-3.552 \cdot 10^{-5}$	$7.901 \cdot 10^{-4}$
	10^{-3}	$1.023 \cdot 10^{-4}$	$9.228 \cdot 10^{-4}$	$-4.011 \cdot 10^{-5}$	$7.964 \cdot 10^{-4}$

Table 4: Final sensitivities at time $t = 4.5$ s of the buggy maneuver

The small discrepancies between the final sensitivity values can be attributed to the larger dissipation of the ALI3-P formulation, resulting in a slight timing offset between the motion computed by both formulations.

7 Conclusions

The present paper reports the sensitivity equations that correspond to the index-3 augmented Lagrangian formulation with velocity and acceleration projections (ALI3-P), for multibody systems with holonomic and nonholonomic constraints. The sensitivity equations were formulated as a Tangent Linear Model (TLM) for the Newton-Raphson iterative solution of the dynamics at the configuration level, plus two additional nonlinear systems of equations for the velocity and acceleration projections. The algorithm equations can be combined with numerical integration formulas to deliver the sensitivities of the generalized coordinates as the solution of a system of linear equations; the sensitivities of the generalized velocities and accelerations are subsequently obtained solving the systems of equations that result from the differentiation of the projections equations with respect to the parameters.

The proposed method was validated with the sensitivity analysis of three test problems. The

first one was a five-bar linkage with linear springs, which had been previously used in the literature as test problem for other sensitivity formulations. The second problem consisted of a two-mass system that featured a nonholonomic constraint and highlighted the relevance of the velocity and acceleration projections for the method to yield correct results. The ALI3-P formulation showed a more robust behavior in both test cases, delivering correct results while decreasing the effort associated with tuning the penalty and other parameters required by similar formulations. Moreover, the computational performance of the ALI3-P was tested in the sensitivity analysis of a full-scale vehicle model. The results confirmed the ability of the method to evaluate correct sensitivity values of complex systems in an efficient way.

Acknowledgements

The support of the Spanish Ministry of Economy and Competitiveness (MINECO) under project DPI2016-81005-P, the Galician Government through grant ED431B2016/031, and the post-doctoral research contract Juan de la Cierva No. JCI-2012-12376 is greatly acknowledged.

References

[1] Anderson, K.S., Hsu, Y.: Analytical fully-recursive sensitivity analysis for multibody dynamic chain systems. Multibody System Dynamics **8**, 1–27 (2002). DOI 10.1023/A:1015867515213

[2] Banerjee, J.M., McPhee, J.: Symbolic sensitivity analysis of multibody systems. In: J.C. Samin, P. Fisette (eds.) Multibody Dynamics. Computational methods and applications, *Computational Methods in Applied Sciences*, vol. 28, chap. Symbolic Sensitivity Analysis of Multibody Systems, pp. 123–146. Springer (2013). DOI 10.1007/978-94-007-5404-1_6

[3] Bauchau, O.A., Laulusa, A.: Review of contemporary approaches for constraint enforcement in multibody systems. Journal of Computational and Nonlinear Dynamics **3**(1), 011,005–011,005 (2007). DOI 10.1115/1.2803258

[4] Baumgarte, J.: Stabilization of constraints and integrals of motion in dynamical systems. Computer Methods in Applied Mechanics and Engineering **1**(1), 1–16 (1972). DOI 10.1016/0045-7825(72)90018-7

[5] Bayo, E., García de Jalon, J., Serna, M.: A modified Lagrangian formulation for the dynamic analysis of constrained mechanical systems. Computer Methods in Applied Mechanics and Engineering **71**(2), 183–195 (1988)

[6] Bayo, E., Ledesma, R.: Augmented Lagrangian and mass-orthogonal projection methods for constrained multibody dynamics. Nonlinear Dynamics **9**(1-2), 113–130 (1996). DOI 10.1007/BF01833296

[7] Bestle, D., Seybold, J.: Sensitivity analysis of constrained multibody systems. Archive of Applied Mechanics **62**, 181–190 (1992). DOI 10.1007/BF00787958

[8] Brenan, K., Campbell, S., Petzold, L.: Numerical Solution of Initial-Value Problems in Differential-Algebraic Equations. North-Holland, New York (1989)

[9] Callejo, A.: Dynamic response optimization of vehicles through efficient multibody formulations and automatic differentiation techniques. Ph.D. thesis, Escuela Técnica Superior de Ingenieros Industriales. Universidad Politécnica de Madrid (2013)

[10] Callejo, A., García de Jalón, J., Luque, P., Mántaras, D.A.: Sensitivity-based, multi-objective design of vehicle suspension systems. Journal of Computational and Nonlinear Dynamics **10**(3), 031,008 (2015). DOI 10.1115/1.4028858

[11] Cao, Y., Li, S., Petzold, L.: Adjoint sensitivity analysis for differential-algebraic equations: algorithms and software. Journal of Computational and Applied Mathematics **149**(1), 171–191 (2002). DOI 10.1016/S0377-0427(02)00528-9

[12] Chang, C.O., Nikravesh, P.E.: Optimal design of mechanical systems with constraint violation stabilization method. Journal of Mechanisms, Transmissions and Automation in Design **107**(4), 493–498 (1985). DOI 10.1115/1.3260751

[13] Cuadrado, J., Cardenal, J., Morer, P., Bayo, E.: Intelligent simulation of multibody dynamics: Space-state and descriptor methods in sequential and parallel computing environments. Multibody System Dynamics **4**(1), 55–73 (2000). DOI 10.1023/A:1009824327480

[14] Cuadrado, J., Gutiérrez, R., Naya, M., Morer, P.: A comparison in terms of accuracy and efficiency between a MBS dynamic formulation with stress analysis and a non-linear FEA

code. International Journal for Numerical Methods in Engineering **51**(9), 1033–1052 (2001). DOI 10.1002/nme.191

[15] Dias, J., Pereira, M.: Sensitivity analysis of rigid-flexible multibody systems. Multibody System Dynamics **1**, 303–322 (1997). DOI 10.1023/A:1009790202712

[16] Dopico, D., González, F., Cuadrado, J., Kövecses, J.: Determination of holonomic and nonholonomic constraint reactions in an index-3 augmented Lagrangian formulation with velocity and acceleration projections. Journal of Computational and Nonlinear Dynamics **9**(4), 041,006 (2014). DOI 10.1115/1.4027671

[17] Dopico, D., Luaces, A., González, M., Cuadrado, J.: Dealing with multiple contacts in a human-in-the-loop application. Multibody System Dynamics **25**(2), 167–183 (2011). DOI 10.1007/s11044-010-9230-y

[18] Dopico, D., Luaces, A., Lugrís, U., Saura, M., González, F., Sanjurjo, E., Pastorino, R.: Mbslim: Multibody systems in laboratorio de ingeniería mecánica (2009-2016). URL http://lim.ii.udc.es/MBSLIM

[19] Dopico, D., Sandu, A., Sandu, C., Zhu, Y.: Sensitivity analysis of multibody dynamic systems modeled by odes and daes. In: Z. Terze (ed.) Multibody Dynamics. Computational Methods and Applications, *Computational Methods in Applied Sciences*, vol. 35, chap. Sensitivity Analysis of Multibody Dynamic Systems Modeled by ODEs and DAEs, pp. 1–32. Springer (2014). DOI 10.1007/978-3-319-07260-9

[20] Dopico, D., Zhu, Y., Sandu, A., Sandu, C.: Direct and adjoint sensitivity analysis of ordinary differential equation multibody formulations. Journal of Computational and Nonlinear Dynamics **10**(1), 1–8 (2014). DOI 10.1115/1.4026492

[21] Eich-Soellner, E., Führer, C.: Numerical Methods in Multibody Dynamics. B.G.Teubner Stuttgart (1998)

[22] Flores, P., Machado, M., Seabra, E., Tavares da Silva, M.: A parametric study on the Baumgarte stabilization method for forward dynamics of constrained multibody systems. Journal of Computational and Nonlinear Dynamics **6**(1), paper 011,019 (2011). DOI 10.1115/1.4002338

[23] García de Jalón, J., Bayo, E.: Kinematic and dynamic simulation of multibody systems: The real-time challenge. Springer-Verlag, New York (USA) (1994)

[24] García Orden, J.: Energy considerations for the stabilization of constrained mechanical systems with velocity projection. Nonlinear Dynamics **60**, 49–62 (2010). DOI 10.1007/s11071-009-9579-8

[25] García Orden, J., Conde, S.: Controllable velocity projection for constraint stabilization in multibody dynamics. Nonlinear Dynamics **68**, 245–257 (2012). DOI 10.1007/s11071-011-0224-y

[26] García Orden, J., Dopico, D.: On the stabilizing properties of energy-momentum integrators and coordinate projections for constrained mechanical systems. In: J. J.C. Garcia Orden, J. Cuadrado (eds.) Multibody Dynamics: Computational Methods and Applications, *Computational Methods in Applied Sciences*, vol. 4, chap. On the Stabilizing Properties of Energy-Momentum Integrators and Coordinate Projections for Constrained Mechanical Systems, pp. 49–68. Springer (2007). DOI 10.1007/978-1-4020-5684-0_3

[27] Gear, C., Leimkuhler, B., Gupta, G.: Automatic integration of Euler-Lagrange equations with constraints. Journal of Computational and Applied Mathematics **12–13**, 77–90 (1985). DOI http://dx.doi.org/10.1016/0377-0427(85)90008-1

[28] Géradin, M., Cardona, A.: Flexible Multibody Dynamics. A Finite Element Approach. John Wiley & Sons Ltd, Chinchester (England) (2001)

[29] González, F., Dopico, D., Pastorino, R., Cuadrado, J.: Behaviour of augmented Lagrangian and Hamiltonian methods for multibody dynamics in the proximity of singular configurations. Nonlinear Dynamics **85**(3), 1491–1508 (2016). DOI 10.1007/s11071-016-2774-5

[30] González, F., Kövecses, J.: Use of penalty formulations in dynamic simulation and analysis of redundantly constrained multibody systems. Multibody System Dynamics **29**(1), 57–76 (2013). DOI 10.1007/s11044-012-9322-y

[31] Gutiérrez-López, M.D., Callejo, A., García de Jalón, J.: Computation of independent sensitivities using Maggi's formulation. In: The 2nd Joint International Conference on Multibody System Dynamics. Stuttgart, Germany (2012)

[32] Haug, E.: Computer aided optimal design: structural and mechanical systems, chap. Design sensitivity analysis of dynamic systems, pp. 705–755. No. 27 in NATO ASI series. Series F, Computer and systems sciences. Springer-Verlag (1987). DOI 10.1007/978-3-642-83051-8_22

[33] Haug, E.J.: Computer Aided Kinematics and Dynamics of Mechanical Systems: Basic Methods. Allyn and Bacon. Prentice Hall College Div, Boston (1989)

[34] Kane, T.R., Levinson, D.A.: Dynamics – Theory and Applications. McGraw-Hill, New York (1985)

[35] Naya, M., Cuadrado, J., Dopico, D., Lugris, U.: An efficient unified method for the combined simulation of multibody and hydraulic dynamics: Comparison with simplified and co-integration approaches. Archive of Mechanical Engineering **58**(2), 223–243 (2011). DOI 10.2478/v10180-011-0016-4

[36] Newmark, N.M.: A method of computation for structural dynamics. Journal of the Engineering Mechanics Division, ASCE **85**(EM3), 67–94 (1959)

[37] Pagalday, J., Aranburu, I., Avello, A., García de Jalón, J.: Multibody dynamics optimization by direct differentiation methods using object oriented programming. In: IUTAM symposium on optimization of mechanical systems, pp. 213–220. Springer (1996). DOI 10.1007/978-94-009-0153-7_27

[38] Pagalday, J., Avello, A.: Optimization of multibody dynamics using object oriented programming and a mixed numerical-symbolic penalty formulation. Mechanism and Machine Theory **32**(2), 161–174 (1997). DOI 10.1016/S0094-114X(96)00037-7

[39] Pastorino, R., Sanjurjo, E., Luaces, A., Naya, M.A., Desmet, W., Cuadrado, J.: Validation of a real-time multibody model for an X-by-wire vehicle prototype through field testing. Journal of Computational and Nonlinear Dynamics **10**(3), 031,006 (2015). DOI 10.1115/1.4028030

[40] Paul, B., Krajcinovic, D.: Computer analysis of machines with planar motion. ASME Journal of Applied Mechanics **37**(3), 697–712 (1970). DOI 10.1115/1.3408599

[41] Schaffer, A.: Stability of the adjoint differential-algebraic equation of the index-3 multibody system equation of motion. SIAM Journal on Scientific Computing **26**(4), 1432–1448 (2005). DOI 10.1137/030601983

[42] Schaffer, A.: Stabilized index-1 differential-algebraic formulations for sensitivity analysis of multi-body dynamics. Proceedings of the Institution of Mechanical Engineers Part K-Journal of Multi-Body Dynamics **220**(3), 141–156 (2006). DOI 10.1243/1464419JMBD62

[43] Schiehlen, W.: Multibody system dynamics: Roots and perspectives. Multibody System Dynamics **1**(2), 149–188 (1997). DOI 10.1023/A:1009745432698

[44] Serna, M.A., Avilés, R., García de Jalón, J.: Dynamic analysis of plane mechanisms with lower pairs in basic coordinates. Mechanism and Machine Theory **17**(6), 397–403 (1982). DOI 10.1016/0094-114X(82)90032-5

[45] Sheth, P., Uicker, J.: IMP (integrated mechanism program): A computer-aided design analysis system for mechanisms and linkages. Journal of Engineering for Industry **94**, 454–464 (1972). DOI 10.1115/1.3428176

[46] Smith, D., Chace, M., Rubens, A.: The automatic generation of a mathematical model for machinery systems. Journal of Engineering for Industry. **95**, 629–635 (1973). DOI 10.1115/1.3438201

[47] Wehage, R., Haug, E.: Generalized coordinate partitioning for dimension reduction in analysis of constrained mechanical systems. Journal of Mechanical Design **104**(1), 247–255 (1982). DOI 10.1115/1.3256318

[48] Zhu, Y., Dopico, D., Sandu, C., Sandu, A.: Dynamic response optimization of complex multibody systems in a penalty formulation using adjoint sensitivity. Journal of Computational and Nonlinear Dynamics **10**(3), 1–9 (2015). DOI 10.1115/1.4029601. URL http://dx.doi.org/10.1115/1.4029601